Distinct lysosomal dysfunction patterns of GRN deficiency in the CNS implicate progranulin in cell type–specific protein sorting

Gordon C Werthmann[1,2,5] and Joachim Herz[1,2,3,4,6]

[1] Department of Molecular Genetics, University of Texas Southwestern Medical Center, Dallas, TX, USA.

[2] Center for Translational Neurodegeneration Research, Dallas, TX, USA.

[3] Department of Neuroscience, University of Texas Southwestern Medical Center, Dallas, TX, USA.

[4] Department of Neurology and Neurotherapeutics, University of Texas Southwestern Medical Center, Dallas, TX, USA.

[5] Corresponding author: gwerthmann@mgb.org

[6] Corresponding author: Joachim.herz@utsouthwestern.edu

Keywords: Neurodegeneration, Neural Ceroid Lipofuscinosis, Frontotemporal Lobar Degeneration, Lysosomal Proteome, Endo-lysosomal Dysfunction

Abstract

Loss-of-function mutations in Progranulin (*GRN*) cause neuronal ceroid lipofuscinosis (NCL) and hereditary frontotemporal dementia, presumably through lysosomal dysfunction. Lysosomes are key metabolic organelles whose functions vary widely depending on their cell type of origin. These functional variations are driven by the lysosomal proteome, yet whether progranulin deficiency alters the lysosomal composition of the mammalian brain in a cell type-specific manner has not been tested. To answer this unknown, we used cell type-specific LysoIP to perform tandem-mass-tag mass-spectrometry and detected distinct aberrant proteomic signatures in progranulin-deficient astrocytes, neurons, and microglia, indicating cell type-specific dysregulation of key lysosomal proteins with crucial functions in sphingolipid metabolism and lysosome organization. These proteins markedly differed from progranulin-deficient RNAseq data sets, suggesting progranulin regulates lysosomal composition through post-translational mechanisms including the sorting of nascent proteins to the lysosome. Validation experiments confirmed that Mfsd8 and Ppt1, proteins whose mutations on their own cause NCL, were essentially absent from progranulin-deficient neuronal and microglial lysosomes, respectively. Our findings demonstrate the protein composition of lysosomes are uniquely sensitive to progranulin deficiency in a cell type-specific manner and that progranulin may function as an essential hub for endolysosomal homeostasis.

Introduction

Frontotemporal dementia (FTD) is the second most common form of pre-senile dementia and presents with a myriad of symptoms including behavioral abnormalities, impaired executive function, and aphasia (1, 2). Up to 40% of FTD cases are thought to be inherited, and haploinsufficiency of the *GRN* gene on chromosome 17 is one of the most common causes of familial FTD, termed GRN-FTD (3, 4). Patients with GRN-FTD primarily develop the behavioral variant of FTD, and on autopsy, the brains of these patients commonly contain TDP-43 aggregates. *GRN* codes for the protein progranulin, a lysosome resident protein comprised of 7 disulfide bond-rich, full length granulin domains and an N-terminal half-granulin domain. While targeted to the lysosome through various membrane protein interactions (5, 6), progranulin is also known to be secreted into the extracellular space where it is either cleaved into individual granulins or endocytosed and delivered to the lysosome through the endocytic pathway (7, 8).

While haploinsufficiency of *GRN* leads to GRN-FTD, homozygous loss of progranulin leads to a classic lysosomal storage disorder termed CLN11 (neuronal ceroid lipofuscinosis 11) (9). Unlike most proteins associated with lysosomal storage disorders, progranulin or granulins do not appear to have any catalytic function and thus likely function as regulatory proteins within the lysosome. The exact nature of how progranulin regulates the lysosomes, and why loss of progranulin leads to a lysosomal storage disorder are currently unknown, but the links between progranulin and lysosomal function are evident. Loss of progranulin leads to impaired cathepsin D activity (10, 11), aberrant lysosomal lipid composition including decreased levels of the lysosome-specific lipid BMP (bis(monoacylglycerol)phosphate), increased levels of tri-acyl glycerol species (12-14), lysosomal alkalinization (15), and impaired lysosomal protein content *in vitro* (16) and *in vivo (17)*. Progranulin deficiency also activates the CLEAR (coordinated lysosomal expression and regulation) gene network by increasing the nuclear localization of the lysosomal gene master regulator TFEB (transcription factor EB) (18, 19).

69 Progranulin has further been shown to regulate various cellular functions including neurite
70 outgrowth, immune regulation, and cell migration (20-24). As both a resident lysosomal protein
71 as well as a secreted protein, the mechanism by which progranulin effects such a large range of
72 cellular processes has yet to be fully determined. However, previous work has demonstrated non-
73 secreted, lysosome-targeted progranulin recapitulates the excitotoxic protective effects of wild
74 type progranulin on cultured neurons (25). This suggests the lysosomal function of progranulin is
75 – at least in part – responsible for the non-lysosomal effects of progranulin. Loss of progranulin
76 also leads to a proinflammatory phenotype, and microglia-selective loss of progranulin can
77 recapitulate several phenotypes seen in whole brain progranulin deficiency (26). Progranulin
78 deficient mice demonstrate microgliosis and increased secretion of inflammatory cytokines such
79 as C1qa and C3 (22). *In vitro*, these microglia are sufficient to induce aggregation of TDP-43 in
80 co-cultured neurons (27).

81 How progranulin regulates lysosomal function remains to be understood; however,
82 previous work has demonstrated loss of progranulin leads to aberrations of the lysosomal
83 proteome, dysregulating key lysosomal proteins that are also implicated in lysosomal storage
84 disorders (16, 17). Lysosomes take on unique functions depending on their cell type of origin (28,
85 29), and previous work has demonstrated the cell types of the mammalian brain also have unique
86 lysosomal proteomes (30). We hypothesized that lysosomal proteomes are uniquely sensitive to
87 progranulin in a cell type-dependent manner. In order to test this, we utilized a technology termed
88 LysoTag which allows for the isolation of lysosomes *in vivo* in a cell type-specific manner in order
89 to investigate the effects of progranulin deficiency on the lysosomal proteome (31). The specificity
90 of this technique allowed for precise isolation and investigation of the lysosomal proteome in
91 progranulin-deficient neurons, microglia, and astrocytes, revealing cell-type dependent protein
92 aberrations not evident upon whole brain analysis nor at the transcript level, and demonstrating
93 the ability of progranulin to regulate cell-specific lysosomal protein homeostasis in the mammalian
94 brain.

95

96 **Results**

97

98 LysoIP isolates lysosomes from specific cell types in *Grn* WT, Het, and KO mice

99 In order to investigate the effects of progranulin deficiency on the lysosomal proteome *in*
100 *vivo*, we bred four specific Cre recombinase lines with previously defined TMEM192-3xHA fl/fl
101 (30, 31) and *Grn* KO mouse lines (13). These included *Ubc*-, *Syn*-, *Cx3cr1*-, and *Aldh1l1-Cre* lines
102 for pancellular, neuron-, microglia-, and astrocyte-specific LysoIP, respectively (Figure 1a). LysoIP
103 was performed on the brains of 2 to 3-month-old *Ubc*-, *Syn*-, and *Cx3cr1-Cre* mice or 6-month-
104 old *Aldh1l1-Cre* mice. 6-month-old *Aldh1l1-Cre* mice were used, because progranulin was
105 undetectable in any 3-month-old *Aldh1l1-Cre* mouse LysoIP sample including those derived from
106 *Grn* WT mice. This is in line with progranulin being primarily expressed in neurons and microglia
107 (32). Protein concentrations were normalized prior to tandem mass tag mass spectrometry (TMT-
108 MS). Splenic macrophage-derived lysosomes were also obtained from *Cx3cr1-Cre* mice to further
109 characterize the effect of progranulin loss on immune cell lysosomes. Western blot verification
110 demonstrated reliable and specific isolation of lysosomes from all four Cre lines (Figure 1b-e).
111 Interestingly, in *Cx3cr1-Cre* LysoIP samples, Lamp1, a marker for lysosomal membranes,
112 demonstrated a molecular weight shift from ~75 kDa to ~110 kDa (Figure 1c). This was seen in
113 both whole-cell lysate and LysoIP samples from mouse spleens – an organ primarily comprised
114 of immune cells (Supplemental Figure 1a), suggesting this shift is specific to immune cells and is
115 thus unlikely to be seen in whole-brain lysates. Lamp1 has various glycosylation sites which likely
116 lead to this mass shift (33).

117 After TMT-MS, raw protein intensities were processed and normalized as described in
118 Methods (Supplemental Figure 1b-e). Several thousand proteins were detected in each TMT-MS
119 run (*Ubc-Cre*: 2310 proteins, *Cx3cr1-Cre* (Brain): 2302 proteins, *Cx3cr1-Cre* (Spleen): 1972
120 proteins, *Aldh1l1-Cre*: 2263 proteins, and *Syn-Cre*: 2219 proteins). To ensure stringent analysis

121 of the lysosomal proteome only, LysoIP samples were compared to no *Cre* control samples added
122 to each TMT-MS run (Figure 1f-i, Supplemental Figure 1f), and proteins were only included for
123 further analysis if they were significantly enriched in LysoIP samples compared to no *Cre* controls
124 and if their normalized abundance was at least 1.5x that of no *Cre* controls. This resulted in
125 hundreds of proteins per *Cre* line (*Ubc-Cre*: 332 proteins, *Cx3cr1-Cre* (Brain): 111 proteins,
126 *Cx3cr1-Cre* (Spleen): 147 proteins, *Aldh1l1-Cre*: 285 proteins, and *Syn-Cre*: 295 proteins). Gene
127 ontology analysis of the resultant proteins demonstrated significant enrichment for lysosomal
128 compartments (Figure 1j-m).

129 Between all TMT-MS runs, 526 unique lysosomal proteins were detected in both *Grn* WT
130 and *Grn* KO LysoIP samples. Several of these proteins were shared between at least 2 individual
131 Cre lines; however, 45.4% of all proteins detected were only detected in a single Cre line (Figure
132 1f). This most likely represents a cell type-specific lysosomal proteomic landscape(34). These
133 proteins were then compared between *Grn* WT, *Grn* heterozygous, and *Grn* KO LysoIP samples
134 of the same Cre using ANOVA and multiple comparison correction as outlined in Methods. Any
135 protein with an adjusted p-value < 0.05 was considered significant. Comparing significantly
136 altered proteins between Cre lines, most significantly altered proteins were detected in neuronal
137 lysosomes (*Syn-Cre*) (Figure 1o, j). When comparing the number of significantly altered proteins
138 in individual Cre lines to the total number of proteins detected, microglial and neuronal lysosomes
139 demonstrated the highest percentage of significantly altered proteins (26.1% and 40.0%,
140 respectively) (Supplemental Figure 1h-k). This is consistent with progranulin primarily being
141 expressed in microglia and neurons. Gene ontology analysis of all significantly altered lysosomal
142 proteins across Cre lines – using all 526 lysosomal proteins as background – highlights
143 carbohydrate derivative catabolism, lipid storage, lysosomal organization, glycoprotein
144 catabolism, and cholesterol efflux as some of the most highly enriched cellular processes affected
145 by progranulin deficiency (Figure 1p; Supplemental Table 1).
146

147 Changes to progranulin-deficient lysosomes are not reflected in mRNA or whole-cell lysate
148 changes

149 Comparing *Ubc-Cre*+ *Grn* WT and *Grn* KO samples, progranulin deficiency significantly
150 altered 13/332 proteins with 8 of these proteins being upregulated and 5 downregulated (Figure
151 2a-c; Supplemental Table 2) while lysosomes from *Grn* heterozygous mouse brains did not
152 demonstrate any significant changes (Figure 2b). Proteins associated with endo-lysosomal
153 trafficking such as Tspan7 were significantly upregulated in *Grn* KO *Ubc-Cre* LysoIP samples (35,
154 36). Tspan 7 has also been associated with synaptic transmission(37, 38). Interestingly, Tthy2
155 and Ttyh3 are also significantly upregulated in *Grn* KO *Ubc-Cre* LysoIP samples. Tthy2 was
156 recently shown to interact with ApoE and facilitate endosomal lipid transfer (39). The APOE4 allele
157 is the strongest genetic predictor for Alzheimer's disease (AD), and patients with GRN mutations
158 are also genetically predisposed to AD, suggesting the effect of progranulin deficiency on
159 lysosomal Tthy2 may contribute to this increased risk of developing AD (40, 41).

160 We next compared progranulin-deficient LysoIP samples against TMT-MS results of
161 progranulin-deficient whole brain lysates (Figure 2d-e) (42). 237 proteins were shared between
162 these datasets; however, only progranulin was found to be significantly altered in both LysoIP and
163 whole brain samples. There was overall poor correlation between progranulin-dependent changes
164 from these datasets, suggesting the effects of progranulin deficiency on the lysosomal proteome
165 can primarily only be detected by directly measuring lysosomal proteins as previously reported
166 (43). Further, comparisons between $\log_2$FC's of the 301 proteins detected in both our *Grn* KO
167 LysoIP samples and *Grn* KO RNA-Seq datasets from Evers *et al.* 2017 similarly demonstrate lack
168 of overlap in significantly altered proteins (Figure 2f) (13), and when comparing all proteins
169 detected in *Ubc-Cre* LysoIP samples to their respective mRNA transcripts from whole-brain RNA-
170 Seq data, no significant correlation can is detected (Figure 2g). This implies progranulin deficiency
171 alters the lysosomal proteome at the post-transcriptional level.

172

173 Progranulin deficiency causes minor changes in astrocyte lysosomes

174 Progranulin expression in astrocytes is relatively low compared to other cell types in the
175 brain (32). In fact, TMT-MS analysis of 3-month-old *Aldh1l1-Cre* LysoIP samples did not detect
176 progranulin. However, progranulin was detected in 6-month-old *Aldh1l1-Cre* LysoIP samples, and
177 comparisons of these samples demonstrated 15/285 significantly altered lysosomal proteins
178 between *Grn* WT vs *Grn* KO mouse brains, with 3 being significantly upregulated and 12 being
179 significantly downregulated (Figure 2h-i, Supplemental Table 3). Similar to *Ubc-Cre* experiments,
180 the membrane protein Ttyh2 is upregulated in *Grn* KO astrocyte lysosomes, and several proteins
181 involved in sphingolipid metabolism such as Galc and Gba1 are downregulated (44, 45). Galc
182 and Gba1 mutations have also both been implicated in Parkinsons disease (46, 47).

183

184 Progranulin deficiency dysregulates various disease-related proteins in the neuronal lysosome

185 In contrast to the minimal effect of progranulin loss on *Ubc-Cre*+ and *Aldh1l1-Cre*+ LysoIP
186 samples, progranulin deficiency heavily influences the neuronal lysosomal proteome, leading to
187 118/295 proteins being significantly altered with 59 proteins being upregulated and 59 being
188 downregulated (Figure 3a-b; Supplemental Table 4). PCA demonstrates clear delineation
189 between *Grn* WT and *Grn* KO neuronal lysosomes while *Grn* heterozygous lysosomes are more
190 heterogeneous between samples (Figure 3c). When investigating the cellular functions related to
191 significantly altered proteins in *Grn* KO neuronal lysosomes, gene ontology analysis demonstrates
192 sphingolipid biosynthesis, lipid biosynthesis, and lysosome organization as the most highly
193 enriched terms (Figure 3d; Supplemental Table 5). Proteins associated with ceramide metabolism
194 such as Neu4, Asah1, Asah2, and Gba1 are all downregulated in *Grn* KO neuronal lysosomes
195 (Figure 3e). Key autophagy proteins that are part of mTORC1 including mTor, Mlst8, and Rptor
196 are all significantly upregulated in *Grn* KO neuronal lysosomes while the adaptor proteins
197 Lamtor2, Lamtor4, and the amino acid transporter Slc38a9 are all significantly downregulated(48).

198 This dysregulation may contribute to the impaired autophagy previously described in models of
199 progranulin deficiency (49, 50).

200 Several mitochondrial proteins including Vdac1/2/3 and Samm50 are all upregulated in
201 *Grn* KO neuronal lysosomes (Supplemental Figure 2a) (51-54). Progranulin deficiency has been
202 implicated in mitophagy defects(55, 56), so we performed Seahorse analysis to determine if
203 mitochondria in *Grn* KO mouse brains demonstrated decreased function. We did not observe any
204 overt mitochondrial deficits using this method (Supplemental Figure 2b-c). However, we did detect
205 a significantly decreased NAD+/NADH ratio from *Grn* KO mouse brains compared to *Grn* WT
206 (Supplemental Figure 2d-f). This was driven by both an increase in NADH and a decrease in
207 NAD+ in *Grn* KO mouse brains and demonstrates how progranulin deficiency alters brain energy
208 homeostasis.

209 Mfsd8 was the most significantly downregulated protein between *Grn* WT and *Grn* KO
210 LysoIP samples. Homozygous MFSD8 nonsense mutations lead to a classic lysosomal storage
211 disorder (CLN7), and missense mutations have also been found to be associated with FTD in a
212 small subset of patients (57). Western blot analysis verified Mfsd8 was heavily decreased in *Grn*
213 KO neuronal lysosomes (Figure 3f-g). Mfsd8 was not detected in either astrocyte or microglial
214 LysoIP samples, suggesting it is specific to neuronal lysosomes and thus only regulated by
215 neuronal progranulin.

216 Of the proteins significantly dysregulated in *Grn* KO neuronal lysosomes, 32 of them are
217 known lysosomal proteins associated with known neurologic disorders based on the OMIM
218 database (Figure 3h, Table 1) (34). This includes proteins associated with lysosomal storage
219 disorders such as Mfsd8, Smpd1, Galc, and Asah1 (44, 58-60).

220

221 <u>Progranulin deficiency dysregulates disease-relevant proteins in the microglial lysosome</u>

222 While fewer total lysosomal proteins were detected in *Cx3cr1-Cre* LysoIP samples – likely
223 due to less starting material – several key lysosomal proteins were found to be dysregulated

224 secondary to progranulin deficiency with a total of 29/111 proteins being significantly altered with
225 14 proteins being upregulated and 15 being downregulated (Figure 4a-c; Supplemental Table 6).
226 Based on GO analysis, progranulin deficiency in microglia primarily affects lysosomal proteins
227 associated with lipid catabolism and tissue regeneration, both processes known to be
228 dysregulated in models of progranulin deficiency (13, 61) (Figure 4d; Supplemental Table 7).

229 To test whether the effects of progranulin deficiency on lysosomal protein composition
230 were specific to microglia or were universal to all immune cells, we performed TMT-MS analysis
231 on LysoIP samples derived from spleens of *Cx3cr1-Cre*+; *Grn* WT and KO mice. This analysis
232 revealed several proteins significantly altered in *Grn* KO splenic macrophage lysosomes
233 compared to *Grn* WT (Supplemental Figure 3a-c; Supplemental Table 8). However, when
234 comparing proteins between *Grn* KO microglial and splenic macrophages by principal component
235 analysis, the two tissue types clustered separately (Figure 4e) and several proteins were found
236 to be significantly different (Figure 4f). This suggests the effects of progranulin deficiency on
237 immune cells are in part dependent on the tissue of origin. Of note, Pld4 is significantly
238 downregulated in progranulin deficient microglia (log_2FC = -1.00, adjusted p-value = 0.003). Pld4
239 was recently discovered to be a synthetic protein for BMPs within the lysosomes of immune cells
240 (62). BMPs are also significantly downregulated in models of progranulin deficiency and are key
241 lysosomal lipids that act as mediators of catabolic processes (12, 14). These data suggest loss
242 of BMPs in progranulin deficient brains may be in part secondary to progranulin-dependent Pld4
243 deficiency.

244 We were also interested to test whether the changes we saw in the microglial lysosomal
245 proteome were reflected in microglial RNA-Seq data. To accomplish this, we compared the
246 log2FC's of *Cx3cr1-Cre*+;*Grn* KO LysoIP samples to *Grn* KO mRNA samples from a previously
247 published microglial RNA-Seq datasets (Figure 4g) (63). 80 of the 111 LysoIP proteins were
248 detected in the RNA-Seq dataset. This included 18 proteins that are significantly altered in the
249 *Cx3cr1-Cre* LysoIP dataset. However, the log2FC values of these proteins did not correlate to the

250 log2FC values of their accompanying transcripts (r^2 = 0.029). This suggests the majority of the
251 effects of progranulin deficiency on the microglial lysosomal proteome are not secondary to
252 alterations at the mRNA level.

253 One of the proteins most significantly downregulated in *Grn* KO microglial lysosomes is
254 palmitoyl protein thioesterase 1 (Ppt1). Mutation of this protein leads to neuronal ceroid
255 lipofuscinosis 1 (CLN1), an early onset lysosomal storage disorder with severe symptoms such
256 as microcephaly, hypotonia, and epilepsy (64). Western blot analysis of LysoIP samples from
257 brains of *Cx3cr1-Cre*+, *Syn-Cre*+, and *Ubc-Cre*+ mice demonstrates Ppt1 is effectively absent
258 from microglial lysosomes but not significantly altered in whole-brain or neuronal lysosomes
259 (Figure 4h-k). In our TMT-MS datasets, Ppt1 is significantly down-regulated in *Syn-Cre*+;*Grn* KO
260 LysoIP samples compared to *Grn* WT controls, and while Western blot analysis of these samples
261 does not recapitulate these findings, there is certainly a trend for decreased Ppt1 in *Grn* KO
262 neuronal lysosomes. Regardless, the effect of progranulin deficiency on microglial Ppt1 is much
263 larger than the effect on neuronal Ppt1 in both TMT-MS and western blot analysis.

264 While Ppt1 is absent in *Grn* KO microglial lysosomes, it is plausible progranulin deficiency
265 leads to accumulation of Ppt1 in non-lysosomal compartments. To test this possibility, we isolated
266 microglia and microglial lysosomes from the left and right hemibrains of 9 to 12-month-old *Cx3cr1-*
267 *Cre*+ mice, respectively (see Methods). Western blot analysis of both whole microglial and
268 microglial lysosome samples demonstrated significantly decreased levels of Ppt1 in *Grn* KO mice
269 compared to *Grn* WT (Figure 5l-n). This decrease was not significantly different between whole
270 microglia and microglial lysosomes, suggesting progranulin deficiency does not lead to
271 accumulation of missorted lysosomal proteins but instead causes overall decreases of microglial
272 lysosomal proteins.

273 Progranulin deficiency has also been associated with hyperinflammatory states (24, 65,
274 66). Further, mutations in several other CLN-related proteins – including Ppt1 – have been shown
275 to increase the activation of the cGAS-STING pathway (67, 68). Similarly, loss of another FTD-

276 related protein C9orf72 also leads to increased cGAS-STING signaling (69). Ppt1 has also been
277 shown to remove the palmitoyl moiety from phosphorylated STING in order to abrogate STING
278 activation (70). To determine if progranulin deficiency led to increased STING signaling similar to
279 other CLN genes, we produced *GRN* KO HeLa cells and measured phosphorylated STING as a
280 function of time after activation with the STING agonist diABZI (71). In the presence of prolonged
281 STING activation, p-STING is known to peak and decline as it becomes digested by the
282 lysosome(72). However, in *GRN* KO cells, STING activation (measured by p-STING levels) was
283 significantly prolonged (Supplemental Figure 4a-d). This suggests progranulin deficiency leads to
284 hyperinflammation in part through prolonged activation of the STING pathway potentially caused
285 by decreased Ppt1-mediated pSTING depalmitoylation. Overall, our data indicate progranulin
286 deficiency impairs microglial lysosomal homeostasis leading to a secondary hyperinflammatory
287 state.
288
289 **Discussion**
290 Progranulin deficiency has long been known to affect lysosomal function with loss of
291 progranulin leading to impaired lysosomal size and shape, impaired lysosomal lipid composition,
292 impaired lysosomal pH regulation, and impaired lysosomal protein activity (10, 12-15). Previous
293 work by our lab and others has further shown that progranulin deficiency leads to aberrations of
294 the lysosomal proteome (16, 17, 73). However, the effect of progranulin deficiency on lysosomal
295 composition in the mammalian brain has not been studied in a cell type-dependent manner. To
296 this end, we utilized an immunoprecipitation-based system to isolate lysosomes from specific cell
297 types in *Grn* WT, heterozygous, and KO mouse brains and spleens. TMT-MS analysis of these
298 samples demonstrated that neuronal and microglial lysosomes were most affected by progranulin
299 deficiency; however, progranulin deficiency led to diverging effects between these cell types.
300 When comparing *Grn* KO LysoIP samples, PCA demonstrates clear separation between
301 lysosomes of different cell types (Figure 5a, Supplemental Table 9). Further analysis

302 demonstrates several proteins whose log_2FC's between *Grn* WT and *Grn* KO are significantly
303 different between *Cx3cr1-Cre+* and *Aldh1l1-Cre+*, *Aldh1l1-Cre+* and *Syn-Cre+*, and *Cx3cr1-Cre+*
304 and *Syn-Cre+* (Figure 5b-d. Supplemental Table 10) LysoIP samples.

305 Progranulin deficiency leads to some proteins such as Naaa and Arsg being significantly
306 downregulated in one cell type and unchanged or even upregulated in another; however,
307 comparisons of proteins significantly altered between *Grn* WT and *Grn* KO LysoIP samples in at
308 least one Cre line demonstrate overall trends of most proteins being consistently up- or
309 downregulated between cell types (Figure 5e-f). Despite this, most proteins affected by
310 progranulin deficiency exhibit cell type-specific sensitivities to this deficiency. For instance, Ppt1,
311 while downregulated between *Grn* WT and *Grn* KO LysoIP samples in all cell types, is more
312 downregulated in microglia compared to astrocytes or neurons. In line with these findings, we
313 propose a hypothetical model where certain proteins are either entirely dependent, somewhat
314 dependent, or independent on progranulin for proper localization and/or stability within the
315 lysosome in a cell type-dependent manner (Figure 6). This model is supported by progranulin
316 being found to physically interact with secretory proteins such as the inflammatory mediator
317 sPLA2-IIa as well as the lysosomal proteins Ctsd, Smpd1, and Gba1, the latter two of which are
318 down-regulated in progranulin deficient lysosomes within the mouse brain (11, 74-76). Of note,
319 these protein-protein interaction studies were performed at neutral pH, suggesting they could
320 occur in the less acidic ER or Golgi apparatus.

321 How progranulin affects the lysosomal proteome in a cell type-sensitive manner is not yet
322 understood; however, this could be achieved by composition-dependent multiprotein complex
323 formation or by certain cell types possessing unknown proteins whose functions are redundant to
324 progranulin, while other cell types are entirely dependent on progranulin for lysosomal localization
325 and/or stability of certain lysosomal proteins. This suggests progranulin may function similarly to
326 CLN6 and CLN8, which are responsible for promoting egress of lysosomal proteins from the ER-
327 Golgi complex, or to prosaposin, the precursor for the lysosomal enzyme activating saposins, an

328 established interaction partner for progranulin that is required in precise stoichiometric proportions
329 for efficient transport of progranulin to the lysosome through ternary complexes with Lrp10 or
330 Surf4 (6, 77-79).

331 Endo-lysosomal dysfunction has been implicated not just in GRN-FTD, but in several
332 neurodegenerative disorders such as Alzheimer's disease and Parkinson's disease as well (80).
333 As post-mitotic cells, neurons do not have the ability to dilute impaired lysosomes through cell
334 division. Lysosome membrane repair is also impaired in an age-dependent manner (81). This
335 leads to accumulation of faulty lysosomes in older neurons, impairing proper macromolecule
336 degradation and nutrient signaling. Why some endo-lysosomal defects lead to the accumulation
337 of certain aggregate-prone proteins (e.g., alpha-synuclein, tau, TDP-43, etc.) is yet to be
338 understood, but the correlation between impaired lysosome function and neurodegeneration is
339 well established and may provide a therapeutic avenue for not just GRN-FTD, but for multiple
340 neurodegenerative disorders.

341 Currently, despite progranulin deficiency leading to 20% of familial FTD, there is no
342 approved treatment for GRN-FTD. Considering the vast network of lysosomal proteins affected
343 by progranulin deficiency in a cell-type sensitive manner, progranulin replacement at the protein
344 synthesis level, and not attempts to correct secondary consequences to lysosomal function or
345 composition, may be the best treatment strategy. Several potential treatments including protein
346 replacement, AAV-technologies, biologics, and small molecule inducers of progranulin expression
347 have emerged in both pre-clinical and clinical trials (14, 16, 82-85). Pathological markers of
348 neurodegenerative diseases appear to accumulate well before the onset of symptoms (86-88),
349 and preventive treatment for these disorders, whenever possible, is likely to provide the best
350 protection against neurodegeneration. Because of its familial inheritance pattern, GRN-FTD is a
351 strong candidate for preventive treatment with progranulin-enhancing agents that aim at
352 increasing the expression of the full-length protein form the remaining functional allele to

353 normalize progranulin levels prior to disease onset. This treatment strategy could potentially stave

354 off the lysosomal aberrations seen in progranulin deficiency and even stall disease onset entirely.

355 **Materials used in the study**

356 Antibodies

357 Mouse anti-Golgin 97 Santa Cruz Cat #: sc-73619

358 Rat anti-Lamp1 DSHB Clone 1D4B

359 Rabbit anti-Calreticulin Cell Signaling Cat #: 12238

360 Rabbit anti-Cathepsin B Cell Signaling Cat #: 31718

361 Rabbit anti-CoxIV Cell Signaling Cat #: 4850

362 Rabbit anti-Gm130 Invitrogen Cat #: MA5-35107

363 Rabbit anti-Calnexin Enzo Cat #: ADI-SPA-860

364 Rabbit anti-Cathepsin D Abcam Cat #: ab75852

365 Rabbit anti-Mfsd8 (Cln7) Proteintech Cat #: 24298-1-AP

366 Rabbit anti-Progranulin Sigma Cat #: HPA008763

367 Rabbit anti-Ppt1 (Cln1) Proteintech Cat #: 29653-1-AP

368 Rabbit anti-Psd95 Cell Signaling Cat #: 2507

369 Rabbit anti-Eaat2 Abcam Cat #: ab41621

370 Rabbit anti-Iba1 Wako FujiFilm Cat #: 019-19741

371 Rabbit anti-beta-Actin Abcam Cat #: ab8227

372 Rabbit anti-Sting Cell Signaling Cat #: 13647

373 Rabbit anti-phospho-STING (S366) Cell Signaling Cat #: 19781

374

375 Bacterial and virus strains

376 pX330-U6-Chimeric_BB-CBh-hSpCas9 Addgene Plasmid #: 42230

377

378 Chemicals, peptides, and recombinant proteins

379 Lipofectamine Thermo Scientific Cat #: 11668030

380 diabzi-Sting-Agonist-3-(Hydrochloride) Cayman Chemical Cat #: 28054-NC2223805

381 Rotenone Sigma Cat #: 557368

382 Sodium Succinate Sigma Cat #: S2378

383 Antimycin A Thermo Scientific Cat #: J63522.MA

384 Sodium Ascorbate Sigma Cat #: PHR1279

385 TMPD Sigma Cat #: T7394

386 ADP Sigma Cat #: 01905

387 Oligomycin Sigma Cat #: O4876

388 FCCP Sigma Cat #: C2920

389 Trypsin Thermo Scientific Cat #: 90056

390 Anti-HA Dynabeads Thermo Scientific Cat # 88836

391 Anti-Cd11b MicroBeads Miltenyi Biotec Cat #: 130-093-636

392

393 Critical commercial assays

394 MicroBCA Protein Assay Kit Thermo Scientific Cat #: 23235

395 NAD/NADH Assay Kit Abcam Cat #: ab65348

396

397 Deposited data

398 Mass spectrometry proteomics data (Grn WT vs Het vs KO LysoIP raw data)

399 MassIVE: Dataset accession number: MSV000099828

400 Password: UTSW2025

401 ftp://MSV000099828@massive-ftp.ucsd.edu

402

403 Experimental models: Cell lines

404 HeLa (89) ATCC Cat #: CCL-2

405

406 Experimental models: Organisms/strains

407 C57BL/6 (Grn WT, Het, KO) Evers et al. 2017

408 B6.129S4-Gt(ROSA)26Sortm1(CAG-TMEM192)Dmsa/J Jackson Labs Strain #: 035401

409 B6.Cg-Ndor1Tg(UBC-cre/ERT2)1Ejb/2J Jackson Labs Strain #: 008085

410 B6.Cg-Tg(Syn1-cre)671Jxm/J Jackson Labs Strain #: 003966

411 B6.129P2(C)-Cx3cr1tm2.1(cre/ERT2)Jung/J Jackson Labs Strain #: 020940

412 B6;FVB-Tg(Aldh1l1-cre/ERT2)1Khakh/J Jackson Labs Strain #: 029655

413

414 Oligonucleotides

415 Grn KO gRNA: 5'-GGATCGAGCCTTCACGTTGCAGG-3'

416 Primer: Grn WT For 5'-agtggggctggccacttct-3'

417 Primer: Grn Mut For 5'-aagattcctcgctgggacatg-3'

418 Primer: Grn WT/Mut Rev 5'-gaatgctggtgtcagagggcc-3'

419 Primer: TMEM192-3xHA wt/wt For 5'-CTGGCTTCTGAGGACCG-3' Laqtom et al. 2023

420 Primer: TMEM192-3xHA wt/wt Rev 5'-AATCTGTGGGAAGTCTTGTCC-3' Laqtom et al. 2023

421 Primer: TMEM192-3xHA fl/fl For 5'-TCCTTGGATATCACCCAGAGT-3' Laqtom et al. 2023

422 Primer: TMEM192-3xHA fl/fl Rev 5'-CCACAAAATAACTTTCCCAAGG-3' Laqtom et al. 2023

423 Primer: UBC-/Syn-/Aldh1l1-Cre For 5'-GCTGCCACGACCAAGTGACAGCAATG-3'

424 Primer: UBC-/Syn-/Aldh1l1-Cre Rev 5'- GTAGTTATTCGGATCATCAGCTACAC-3'

425 Primer: Cx3cr1-Cre WT For 5'- GTGGGAAATCTGTTGGTGGTCCTC-3'

426 Primer: Cx3cr1-Cre Mut For 5'- GTTAATGACCTGCAGCCAAG-3'

427 Primer: Cx3cr1-Cre WT/Mut Rev 5'- TAGTCACCCAGACACTCGTTGTCC-3'

428

429 Software and algorithms

430 Prism GraphPad https://www.graphpad.com/features

431 ImageJSchneider et al. https://imagej.net/ij/

432 RStudio Posit Team (2024) http://www.posit.co/

433 Limma Ritchie et al. DOI: 10.18129/B9.bioc.limma

434

435 **Methods**

436 Cell Culture

437 All cell culture reagents and plates were purchased from Corning (Corning, NY, USA). Cells were

438 maintained at 8.8% CO2 at 37 °C. HeLa cells were cultured in high glucose Dulbecco's Modified

439 Eagle's Medium (DMEM) with 10% FCS and Pen/Strep and supplied from ATCC (CCL-2).

440

441 Generation of *GRN* KO HeLa cells

442 HeLa cells were transfected with a plasmid containing both Cas9 and sgRNA targeting the R493

443 region of progranulin as this is one of the most commonly mutated residues(89). Transfection was

444 performed with Lipofectamine 2000 in a ratio of 6:1 (6 μL Lipofectamine: 1 μg DNA). 48-72 hours

445 after transfection, positive cells were selected using puromycin, and individual clones were
446 isolated, grown, and tested for progranulin via western blot.
447
448 STING activation assay
449 HeLa cells were grown in 6-well plates to 80-90% confluence and were treated with 1 μM diABZI
450 added to 1 mL fresh media for 0, 1, 2, 4, 8, or 12 hours at 37°C. At designated timepoints, cells
451 were rinsed three times with cold PBS on ice, and protein was harvested by scraping cells in 100
452 μL lysis buffer. Cells were incubated with lysis buffer for 15 minutes at 4°C, insoluble material was
453 pelleted by centrifugation at 21,130g for 10 minutes at 4°C, and supernatant was moved to fresh
454 tube. STING activation was measured by western blot analysis using antibodies to human
455 phospho-STING (Ser 366) and total STING.
456
457 Generation of Grn;TMEM192-3xHA fl/fl mice and animal husbandry
458 The *Grn* mutant mice were originally obtained from the Farese lab and were propagated for at
459 least 50 generations in the Herz lab. Their generation is previously described(13). Animals were
460 maintained on a C57BL/6 J background by heterozygous intercrossing. *Grn* KO mice were bred
461 with TMEM192-3xHA fl/fl mice obtained from Jackson Labs (Strain #035401)(31). *Grn*
462 KO;TMEM192-HA fl/fl mice were then crossbred with either *Ubc-Cre*^{ERT2} (Jackson Labs Strain
463 #008085), *Syn-Cre* (Jackson Lab Strain #003966), *Cx3cr1-Cre*^{ERT2} (Jackson Labs Strain
464 #020940), or *Aldh1l1-Cre*^{ERT2} (Jackson Labs Strain #029655) mice to establish *Grn* WT,
465 heterozygous, or KO; TMEM192-3xHA fl/fl; Cre+ mice. To induce expression of UBC-, Cx3cr1-,
466 and Aldh1l1-Cre, animals were injected at 8 weeks with tamoxifen (120 mg/kg) for up to 5 days.
467 Animals were maintained on a 12 h light/12-h dark cycle and fed a standard rodent chow diet (Diet
468 7001; Harlan Teklad, Madison, WI) and water ad libitum. No sexual dimorphism of phenotype was
469 observed, and both male and female mice were used for all experiments. All procedures were

470 performed in accordance with the protocols approved by the Institutional Animal Care and Use
471 Committee of the University of Texas Southwestern Medical Center (IACUC APN 2015-101088-
472 G).
473
474 *In vivo LysoIP*
475 For isolation of lysosomes from mouse brain, a similar protocol was used as previously
476 described(31, 34). Each LysoIP was individually completed before the next LysoIP was
477 performed. 2-3-month-old (for *Ubc-Cre*, *Cx3cr1-Cre*, and *Syn-Cre*) or 6-month-old (for *Aldh1l1-*
478 *Cre*) mice were anesthetized with isoflurane and immediately perfused with ice cold PBS (5 mL
479 administered over 4-5 minutes). The brain was removed from the skull, and the olfactory bulbs
480 were removed. Brains were cut into 6 pieces and placed in 950 μL homogenization buffer (PBS
481 + protease inhibitor + phosphatase inhibitor). Brains were homogenized on ice with 25 strokes of
482 plunger, and homogenate was moved to 2 mL microcentrifuge tube. 25 μL of homogenate was
483 moved to separate tube for whole cell lysate. 1 mL of homogenization buffer was added to
484 homogenate to decrease pipetting errors. Insoluble material was spun down at 1000g for 2 min
485 at 4°C. All further steps were performed at 4°C.
486
487 1 mL homogenate was added to 100 μL anti-HA Dynabeads which had been pre-washed in 1 mL
488 cold PBS three times before experiment. Homogenate was incubated with Dynabeads with end-
489 over-end rotation for 15 minutes. After incubation, supernatant was removed from Dynabeads,
490 and Dynabeads were washed with 1 mL homogenization buffer three times. After the third wash,
491 Dynabeads were moved to fresh tube. 180 μL lysis buffer was added to Dynabeads and incubated
492 on ice for 15 minutes. Lysis buffer was removed from Dynabeads and moved into fresh tube.
493 For LysoIP of splenic macrophages, the same procedure was used as for the brain, except mice
494 were not perfused with PBS before dissection of the spleen, and 300 μL homogenization buffer

495 was added to homogenate (as opposed to 1 mL with brain LysoIP). All remaining steps were the
496 same as for brain LysoIP.
497
498 For whole cell lysate, 200 uL lysis buffer was added to lysate and incubated with end-over-end
499 rotation for 15 minutes. Insoluble material was spun down at 21,130g for 10 min at 4°C. Lysate
500 was moved to fresh tube, and both lysate and LysoIP were stored at -80°C until downstream
501 applications.
502
503 Tandem mass tag mass spectrometry
504 Sample concentrations were measured by micro-BCA assay and normalized to sample with
505 lowest concentration. Samples were dried for 30 min in a SpeedVac, after which 40 µl of 5% SDS
506 was added to each. Samples were then reduced with TCEP and alkylated with iodoacetamide in
507 the dark. Each sample was loaded onto an S-Trap Micro (Protifi), following which 2 µg of trypsin
508 (Pierce) was added and allowed to digest overnight at 37 °C. Peptides were eluted and dried in a
509 SpeedVac, then were reconstituted in 21 µl of 50 mM TEAB buffer. Samples were then each
510 labeled with 4 µl of TMTpro 16plex reagent (ThermoFisher, Waltham, MA, USA, A44520) and
511 quenched with 2 µl of 5% hydroxylamine and combined in equal peptide amount based on
512 NanoDrop A205 reading. These mixtures were dried in a SpeedVac and reconstituted in 2%
513 acetonitrile, 0.1% TFA buffer.
514
515 Peptides were analyzed on a Thermo Orbitrap Eclipse MS system coupled to an Ultimate 3000
516 RSLC-Nano liquid chromatography system. Samples were injected onto a 75 um i.d., 75-cm long
517 EasySpray column (Thermo) and eluted with a gradient from 0-28% buffer B over 180 min at a
518 flow rate of 250 nL/min. Buffer A contained 2% (v/v) ACN and 0.1% formic acid in water, and buffer
519 B contained 80% (v/v) ACN, 10% (v/v) trifluoroethanol, and 0.1% formic acid in water. at a flow
520 rate of 250 nl/min. Spectra were continuously acquired in a data-dependent manner throughout

521 the gradient, acquiring a full scan in the Orbitrap (at 120,000 resolution with a standard AGC
522 target) followed by MS/MS scans on the most abundant ions in 2.5 s in the ion trap (turbo scan
523 type with an intensity threshold of 5,000, CID collision energy of 35%, standard AGC target,
524 maximum injection time of 35 ms and isolation width of 0.7 m/z). Charge states from 2-6 were
525 included. Dynamic exclusion was enabled with a repeat count of 1, an exclusion duration of 25 s
526 and an exclusion mass width of ± 10 ppm. Real-time search was used for selection of peaks for
527 SPS-MS3 analysis, with searched performed against a list of proteins from the mouse reviewed
528 protein database from UniProt. Up to 2 missed tryptic cleavage was allowed, with
529 carbamidomethylation (+57.0215) of cysteine and TMTpro reagent (+304.2071) of lysine and
530 peptide N-termini used as static modifications and oxidation (+15.9949) of methionine used as a
531 variable modification. MS3 data were collected for up to 10 MS2 peaks which matched to
532 fragments from the real-time peptide search identification, in the Orbitrap at a resolution of 50,000,
533 HCD collision energy of 65% and a scan range of 100–500.
534
535 Protein identification and quantification were done using Proteome Discoverer v.3.0 SP1
536 (Thermo). Raw MS data files were analyzed against the mouse reviewed protein database from
537 UniProt. Both Comet and SequestHT with INFERYS Rescoring were used, with
538 carbamidomethylation (+57.0215) of cysteine and TMTpro reagent (+304.2071) of lysine and
539 peptide N-termini used as static modifications and oxidation (+15.9949) of methionine used as a
540 variable modification. Reporter ion intensities were reported, with further normalization performed
541 by using the total intensity in each channel to correct discrepancies in sample amount in each
542 channel. A co-isolation threshold of 75% and an SPS Mass Matches threshold of 65% was used,
543 and the false-discovery rate (FDR) cutoff was 1% for all peptides.
544
545 <u>Analysis of TMT-MS results</u>

546 For each TMT-MS run, at least one sample from a Cre- mouse was included as a negative control.
547 All samples were normalized to total protein abundance. LysoIP samples were compared to the
548 Cre- control by one-sample t-test followed by Benjamini-Hochberg procedure with FDR set at
549 0.05. Proteins were only included in downstream analysis if they were significantly different
550 compared to Cre- control, had an average $\log_2$FC value > 0.58 compared to Cre- control, and all
551 individual LysoIP sample intensities were greater than no Cre control. Normalized abundances of
552 the Cre- controls were subtracted from the normalized abundances of each sample. Protein
553 quantities were log2 transformed, and the median quantity of protein intensities for each LysoIP
554 sample was subtracted from individual protein intensities to account for differences in cell number
555 and LysoIP efficiency. Differential protein abundance was determined using an ANOVA test
556 applied to the normalized protein quantities using limma(90, 91). Correction for multiple testing
557 was performed using the Benjamini Hochberg method with an FDR set at 0.05. Any protein with
558 adjusted p-value < 0.05 was considered significant. Gene ontology analysis was performed using
559 ShinyGO (92) to compare LysoIP samples and Cre- controls or Metascape to compare *Grn* WT
560 and *Grn* KO LysoIP samples. For ShinyGO, all proteins detected in a single TMT-MS run were
561 used as background proteins to determine enrichment of lysosomal proteins. For Metascape, all
562 526 proteins detected as LysoIP proteins after filtering were included as background.
563
564 Western blotting
565 For STING activation assay, cell lysate was first normalized to match lowest concentration as
566 determined by Lowry assay. For all western blotting (except for Mfsd8 immunoblotting), 5x sample
567 buffer was added per sample, and samples were boiled at 95°C for 10 minutes. 10-14 µl per
568 sample was added to pre-cast gel, and electrophoresis was performed at 120V for 70-90 minutes.
569 Samples were transferred to 0.22 µm nitrocellulose membranes using Bio-Rad semi-dry transfer
570 (25V, 1.3-2.5A, 15 minutes). Membranes were blocked with 5% milk in TBS-T and incubated with
571 primary antibody in 3% BSA in TBS-T + 0.02% NaN_3 either at room temperature for 60 minutes

572 or overnight at 4°C. Membranes were rinsed in TBS-T, and secondary was applied for 60 minutes
573 in 5% milk TBS-T. Membranes were rinsed in TBS-T and either imaged using Licor or ECL.
574
575 For Mfsd8 immunoblotting, 5x sample buffer was added to samples and were heated at 37°C for
576 10 minutes. Samples were run on pre-cast gels as previously described and were transferred to
577 0.22 µm PVDF membranes using wet transfer apparatus (40V overnight at 4°C). Membranes
578 were blocked with 5% milk in TBS-T and incubated with primary antibody in 3% BSA in TBS-T +
579 0.02% NaN_3 overnight at 4°C. Membranes were rinsed in TBS-T, and secondary was applied for
580 60 minutes in 5% milk TBST. Membranes were rinsed in TBS-T and imaged using ECL.
581
582 Isolation of microglia
583 Microglia were isolated from *Grn;TMEM192-3xHA fl/fl;Cx3cr1-Cre*^{ERT2} was performed on 10-12-
584 month-old mice. Mice were anesthetized with isoflurane and perfused with ice cold PBS (10 mL
585 delivered over 4-5 minutes). Brain was harvested and left and right hemibrains were separated.
586 LysoIP was immediately performed on left hemibrain while right hemibrain was left in dissociation
587 buffer on ice. No more than 4 LysoIPs were performed before microglial isolation was performed.
588 To isolate single cell solution, hemibrains were dissociated by mincing tissue in dissociation buffer
589 on ice until no pieces larger than 1 mm remained. Tissue was moved to 50 mL conical tube and
590 rocked at 37°C for 30 minutes. Dissociated tissue was pressed through pre-wet 70 µm nylon filter
591 using rubber end of a syringe plunger. 2 mL sample preparation media was used to rinse
592 remaining cells through filter. Suspension was centrifuged for at 300g for 10 minutes at 4°C with
593 brake set to low. Supernatant was removed, and cell pellet was resuspended in 4 mL 30% percoll
594 solution. Solution was transferred to 15 mL conical tube and spun at 700g for 10 minutes at room
595 temperature with brake set to zero. Upper myelin layer was removed with 5 mL serologic pipette,
596 and remainder of supernatant was removed. Cells were resuspended in 1 mL sample preparation

597 media, and suspension was moved to fresh tube. Suspension was spun down at 300g for 10
598 minutes at 4°C with brake set to low. Supernatant was removed.
599
600 To isolate microglia, pellet was resuspended in 135 μL MACS buffer and 15 μL CD11b beads and
601 was incubated on ice for 15 minutes. 1 mL of MACS buffer was added, and sample was
602 centrifuged at 300g for 10 minutes at 4°C. 70 μm pre-wet nylon filter was placed on LS columns,
603 and both were attached to MACS magnetic stand. Column was prewet with 3 mL MACS buffer.
604 Supernatant was removed from pellet, and pellet was resuspended in 500 μL MACS buffer.
605 Sample was run over column. Tube was rinsed with 2 mL MACS buffer, and rinse was also run
606 over column. 3 mL MACS buffer was run over column.
607
608 Column was removed from magnet, 5 mL MACS buffer was added, and buffer was immediately
609 plunged into fresh tube. This was repeated with another 5 mL MACS buffer. This tube now
610 contained isolated microglia. Cells were spun at 300g for 10 minutes at 4°C with low brake.
611 Supernatant was removed, and pellet was resuspended in 50 μL lysis buffer.
612
613 NAD+/NADH Assay
614 Procedure is described on Abcam website for kit (Cat# ab65348). In brief, ~20 mg whole brain
615 from fasted mice was homogenized in 400 μL Extraction Buffer in Dounce homogenizer (40
616 passes). Samples were centrifuged for 5 minutes 4°C at top speed. Supernatant was passed
617 through a 10 kDa spin column (Millipore Sigma) 30 minutes 4°C at 14,000g to remove NAD-
618 consuming enzymes. Half of sample was reserved as "NAD Total" and half was heated at 60°C
619 for 30 minutes to degrade NAD+ ("NADH"). Added 50 μL sample to 100 μL reaction mix (98 μL
620 NAD cycling buffer + 2 uL NAD cycling enzyme) and incubated at room temp for 5 minutes to
621 convert NAD to NADH. 10 μL of developer solution was added, and colorimetric readout was

622 measured at OD 450 nm at multiple times between 1-4 hours. Samples were compared to 0-100
623 pmol NAD standards. NAD+ was calculated by subtracting NADH from NAD Total, and
624 NAD+/NADH ratios were calculated for each sample.
625
626 Seahorse Assay
627 To isolate mitochondria from 12-month-old *Grn* WT and Grn KO mice, mice were anesthetized
628 with isoflurane and perfused with cold PBS (5 mL over 4-5 minutes). Brains were extracted,
629 minced on ice, and placed in ~10 volumes of isolation buffer. Brains were homogenized by 2-3
630 slow strokes of a Dounce homogenizer. Sample was moved to fresh tube and spun at 800g for
631 10 minutes at 4°C. Supernatant was moved to fresh tube and spun at 8000g for 10 minutes at
632 4°C. Supernatant was removed, pellet was resuspended in 5 mL isolation buffer, and samples
633 were spun at 8000g for 10 minutes for 4°C. Supernatant was removed, and pellet containing
634 mitochondria was resuspended in 100 µL Seahorse buffer. Protein was quantified with BCA, and
635 mitochondria were diluted to a concentration of 100 µg protein/mL. 50 µL (5 µg)
636 mitochondria/sample was transferred to XFe24 Tissue Culture Plate. 4 wells contained 50 µL
637 Seahorse buffer alone as negative controls. Mitochondria were spun down onto plate surface at
638 3600g for 15 minutes at 4°C. 450 µL of starting buffer was added to each well while Seahorse is
639 calibrated according to manual. Starting buffers and injection port compounds are listed below.
640
641 Electron Flow Starting Buffer:
642 Seahorse Buffer + 10 mM pyruvate + 2 mM malate + 4 µM FCCP
643 Electron Flow Injection Ports:
644 Port A: 20 µM (10x) rotenone/injection volume 50 µL
645 Port B: 100 µM (10x) succinate/injection volume 55 µL
646 Port C: 40 µM (10x) actimycin A/injection volume 60 µL
647 Port D: 100mM (10x) ascorbate + 1 mM (10x) TMPD/injection volume 65 µL

648 Electron Coupling Starting Buffer:

649 Seahorse Buffer + 10 mM succinate + 2 μM rotenone

650 Port A: 40 mM (10x) ADP 50 μL

651 Port B: 20 μM (10x) oligomycin 55 μL

652 Port C: 40 μM (10x) FCCP/injection volume 60 μL

653 Port D: 40 μM (10x) antimycin A/injection volume 65 μL

654

655 Quantification and Statistical Analysis

656 Data analysis was conducted using ImageJ (NIH) and Odyssey Imaging Systems (Li-Cor).
657 GraphPad Prism was used for all statistical analysis except TMT-MS analysis which was
658 performed with the limma package which uses the R programming language. Data are displayed
659 as means ± standard errors (SE). Specific statistical tests including number of samples/condition
660 are specified in individual figure legends.

661

662 **Acknowledgments**

663 J. Herz was supported by grants from the NIA (RF1/RF3 AG053391), the NINDS and NIA (R01
664 NS093382 and R01 NS108115), NIAMS (1R43AR081762) and NINDS (1R43AG084450),
665 BrightFocus (A2013524S & A2016396S), the Bluefield Project to Cure FTD, Harrington Discovery
666 Institute (HDI2019-SI-4479), Alzheimer's Association (ABA-22-970304), the Presbyterian Village
667 North Foundation, and the Robert J. Kleberg Jr. & Helen C. Kleberg Foundation, Texas
668 Alzheimer's Research and Care Consortium (TARCC) 1271166 and 1280583. We also thank
669 Tamara Terrones, Brian Emmerson, and Patricia Strackbein for their unrivaled support and brilliant
670 technical assistance.

671

Contributions

GCW and JH planned and conceived the project. GCW performed all experiments, analyzed data, and wrote the manuscript. JH edited the manuscript, obtained funding, and oversaw the execution of the project.

Declaration of Interests

J.H. is a co-founder of Reelin Therapeutics Inc. and coinventor of a patent related to isoxazoles with the ability to increase progranulin expression (Application Number: US15/127,603 and Publication Number: US10149836B2). The remaining authors declare no competing interest.

Data Sharing Statement

All raw mass spec data is shared through the MassIVE proteomics database. Data accession number: MSV000099828

All other raw data are shared through the Texas Data Repository.

688 **References**

689

690 1. Bang J, Spina S, and Miller BL. Frontotemporal dementia. *Lancet.* 2015;386(10004):1672-
691 82.

692 2. Ratnavalli E, Brayne C, Dawson K, and Hodges JR. The prevalence of frontotemporal
693 dementia. *Neurology.* 2002;58(11):1615-21.

694 3. Baker M, Mackenzie IR, Pickering-Brown SM, Gass J, Rademakers R, Lindholm C, et al.
695 Mutations in progranulin cause tau-negative frontotemporal dementia linked to
696 chromosome 17. *Nature.* 2006;442(7105):916-9.

697 4. Rohrer JD, Guerreiro R, Vandrovcova J, Uphill J, Reiman D, Beck J, et al. The heritability
698 and genetics of frontotemporal lobar degeneration. *Neurology.* 2009;73(18):1451-6.

699 5. Hu F, Padukkavidana T, Vaegter CB, Brady OA, Zheng Y, Mackenzie IR, et al. Sortilin-
700 mediated endocytosis determines levels of the frontotemporal dementia protein,
701 progranulin. *Neuron.* 2010;68(4):654-67.

702 6. Zhou X, Sun L, Bastos de Oliveira F, Qi X, Brown WJ, Smolka MB, et al. Prosaposin
703 facilitates sortilin-independent lysosomal trafficking of progranulin. *J Cell Biol.*
704 2015;210(6):991-1002.

705 7. Bai XH, Wang DW, Kong L, Zhang Y, Luan Y, Kobayashi T, et al. ADAMTS-7, a direct
706 target of PTHrP, adversely regulates endochondral bone growth by associating with and
707 inactivating GEP growth factor. *Mol Cell Biol.* 2009;29(15):4201-19.

708 8. Kessenbrock K, Frohlich L, Sixt M, Lammermann T, Pfister H, Bateman A, et al. Proteinase
709 3 and neutrophil elastase enhance inflammation in mice by inactivating antiinflammatory
710 progranulin. *J Clin Invest.* 2008;118(7):2438-47.

711 9. Smith KR, Damiano J, Franceschetti S, Carpenter S, Canafoglia L, Morbin M, et al.
712 Strikingly different clinicopathological phenotypes determined by progranulin-mutation
713 dosage. *Am J Hum Genet.* 2012;90(6):1102-7.

714 10. Valdez C, Wong YC, Schwake M, Bu G, Wszolek ZK, and Krainc D. Progranulin-mediated
715 deficiency of cathepsin D results in FTD and NCL-like phenotypes in neurons derived from
716 FTD patients. *Hum Mol Genet.* 2017;26(24):4861-72.
717 11. Zhou X, Paushter DH, Feng T, Pardon CM, Mendoza CS, and Hu F. Regulation of
718 cathepsin D activity by the FTLD protein progranulin. *Acta Neuropathol.* 2017;134(1):151-
719 3.
720 12. Boland S, Swarup S, Ambaw YA, Malia PC, Richards RC, Fischer AW, et al. Deficiency of
721 the frontotemporal dementia gene GRN results in gangliosidosis. *Nat Commun.*
722 2022;13(1):5924.
723 13. Evers BM, Rodriguez-Navas C, Tesla RJ, Prange-Kiel J, Wasser CR, Yoo KS, et al.
724 Lipidomic and Transcriptomic Basis of Lysosomal Dysfunction in Progranulin Deficiency.
725 *Cell Rep.* 2017;20(11):2565-74.
726 14. Logan T, Simon MJ, Rana A, Cherf GM, Srivastava A, Davis SS, et al. Rescue of a
727 lysosomal storage disorder caused by Grn loss of function with a brain penetrant
728 progranulin biologic. *Cell.* 2021;184(18):4651-68 e25.
729 15. Tanaka Y, Suzuki G, Matsuwaki T, Hosokawa M, Serrano G, Beach TG, et al. Progranulin
730 regulates lysosomal function and biogenesis through acidification of lysosomes. *Hum Mol*
731 *Genet.* 2017;26(5):969-88.
732 16. Tesla R, Guhl C, Werthmann GC, Dixon D, Cenik B, Addepalli Y, et al. Benzoxazole-
733 derivatives enhance progranulin expression and reverse the aberrant lysosomal proteome
734 caused by GRN haploinsufficiency. *Nat Commun.* 2024;15(1):6125.
735 17. Hasan S, Fernandopulle MS, Humble SW, Frankenfield AM, Li H, Prestil R, et al. Multi-
736 modal proteomic characterization of lysosomal function and proteostasis in progranulin-
737 deficient neurons. *Mol Neurodegener.* 2023;18(1):87.
738 18. Butler VJ, Gao F, Corrales CI, Cortopassi WA, Caballero B, Vohra M, et al. Age- and
739 stress-associated C. elegans granulins impair lysosomal function and induce a

740 compensatory HLH-30/TFEB transcriptional response. *PLoS Genet.*
741 2019;15(8):e1008295.
742 19. Tanaka Y, Matsuwaki T, Yamanouchi K, and Nishihara M. Increased lysosomal biogenesis
743 in activated microglia and exacerbated neuronal damage after traumatic brain injury in
744 progranulin-deficient mice. *Neuroscience.* 2013;250:8-19.
745 20. Van Damme P, Van Hoecke A, Lambrechts D, Vanacker P, Bogaert E, van Swieten J, et
746 al. Progranulin functions as a neurotrophic factor to regulate neurite outgrowth and
747 enhance neuronal survival. *J Cell Biol.* 2008;181(1):37-41.
748 21. Gass J, Lee WC, Cook C, Finch N, Stetler C, Jansen-West K, et al. Progranulin regulates
749 neuronal outgrowth independent of sortilin. *Mol Neurodegener.* 2012;7:33.
750 22. Lui H, Zhang J, Makinson SR, Cahill MK, Kelley KW, Huang HY, et al. Progranulin
751 Deficiency Promotes Circuit-Specific Synaptic Pruning by Microglia via Complement
752 Activation. *Cell.* 2016;165(4):921-35.
753 23. He Z, Ismail A, Kriazhev L, Sadvakassova G, and Bateman A. Progranulin (PC-cell-
754 derived growth factor/acrogranin) regulates invasion and cell survival. *Cancer Res.*
755 2002;62(19):5590-6.
756 24. Gillett DA, Wallings RL, Uriarte Huarte O, and Tansey MG. Progranulin and GPNMB:
757 interactions in endo-lysosome function and inflammation in neurodegenerative disease. *J*
758 *Neuroinflammation.* 2023;20(1):286.
759 25. Davis SE, Roth JR, Aljabi Q, Hakim AR, Savell KE, Day JJ, et al. Delivering progranulin to
760 neuronal lysosomes protects against excitotoxicity. *Journal of Biological Chemistry.*
761 2021;297(3).
762 26. Martens LH, Zhang J, Barmada SJ, Zhou P, Kamiya S, Sun B, et al. Progranulin deficiency
763 promotes neuroinflammation and neuron loss following toxin-induced injury. *J Clin Invest.*
764 2012;122(11):3955-9.

765 27. Zhang J, Velmeshev D, Hashimoto K, Huang YH, Hofmann JW, Shi X, et al. Neurotoxic
766 microglia promote TDP-43 proteinopathy in progranulin deficiency. *Nature.*
767 2020;588(7838):459-65.
768 28. Iyer H, Shen K, Meireles AM, and Talbot WS. A lysosomal regulatory circuit essential for
769 the development and function of microglia. *Sci Adv.* 2022;8(35):eabp8321.
770 29. Spencer JI, Sudarikova Y, and Devine MJ. Non-canonical roles of lysosomes in neurons.
771 *Trends Neurosci.* 2025;48(12):1023-38.
772 30. Ghoochani A, Heiby JC, Rawat ES, Medoh UN, Di Fraia D, Dong W, et al. Cell-type
773 resolved protein atlas of brain lysosomes identifies SLC45A1-associated disease as a
774 lysosomal disorder. *Cell.* 2026.
775 31. Laqtom NN, Dong W, Medoh UN, Cangelosi AL, Dharamdasani V, Chan SH, et al. CLN3
776 is required for the clearance of glycerophosphodiesters from lysosomes. *Nature.*
777 2022;609(7929):1005-11.
778 32. Petkau TL, Neal SJ, Orban PC, MacDonald JL, Hill AM, Lu G, et al. Progranulin expression
779 in the developing and adult murine brain. *J Comp Neurol.* 2010;518(19):3931-47.
780 33. Cawley NX, Sojka C, Cougnoux A, Lyons AT, Nicoli ER, Wassif CA, et al. Abnormal LAMP1
781 glycosylation may play a role in Niemann-Pick disease, type C pathology. *PLoS One.*
782 2020;15(1):e0227829.
783 34. Ghoochani A, Heiby JC, Rawat ES, Medoh UN, Di Fraia D, Dong W, et al. Cell-Type
784 Resolved Protein Atlas of Brain Lysosomes Identifies SLC45A1-Associated Disease as a
785 Lysosomal Disorder. *bioRxiv.* 2024.
786 35. Ghossoub R, Chery M, Audebert S, Leblanc R, Egea-Jimenez AL, Lembo F, et al.
787 Tetraspanin-6 negatively regulates exosome production. *Proc Natl Acad Sci U S A.*
788 2020;117(11):5913-22.

789 36. Lee SA, Suh Y, Lee S, Jeong J, Kim SJ, Kim SJ, et al. Functional expression of dopamine
790 D2 receptor is regulated by tetraspanin 7-mediated postendocytic trafficking. *FASEB J.*
791 2017;31(6):2301-13.
792 37. Bassani S, Cingolani LA, Valnegri P, Folci A, Zapata J, Gianfelice A, et al. The X-linked
793 intellectual disability protein TSPAN7 regulates excitatory synapse development and
794 AMPAR trafficking. *Neuron.* 2012;73(6):1143-58.
795 38. Salas IH, Callaerts-Vegh Z, Arranz AM, Guix FX, D'Hooge R, Esteban JA, et al.
796 Tetraspanin 6: A novel regulator of hippocampal synaptic transmission and long term
797 plasticity. *PLoS One.* 2017;12(2):e0171968.
798 39. Sukalskaia A, Karner A, Pugnetti A, Weber F, Plochberger B, and Dutzler R. Interactions
799 between TTYH2 and APOE facilitate endosomal lipid transfer. *Nature.* 2025.
800 40. Reiman EM, Ghisays V, and Langbaum JB. The Risk of Alzheimer Disease in APOE4
801 Homozygotes. *JAMA Neurol.* 2025;82(9):879-80.
802 41. Ingannato A, Bessi V, Chiari A, Salvatori D, Bagnoli S, Bedin R, et al. GRN Missense
803 Variants and Familial Alzheimer's Disease: Two Case Reports. *J Alzheimers Dis.*
804 2023;96(2):767-75.
805 42. Huang M, Modeste E, Dammer E, Merino P, Taylor G, Duong DM, et al. Network analysis
806 of the progranulin-deficient mouse brain proteome reveals pathogenic mechanisms
807 shared in human frontotemporal dementia caused by GRN mutations. *Acta Neuropathol*
808 *Commun.* 2020;8(1):163.
809 43. Singh J, Kaade E, Muntel J, Bruderer R, Reiter L, Thelen M, et al. Systematic Comparison
810 of Strategies for the Enrichment of Lysosomes by Data Independent Acquisition. *Journal*
811 *of Proteome Research.* 2019;19(1):371-81.
812 44. Bongarzone ER, Escolar ML, Gray SJ, Kafri T, Vite CH, and Sands MS. Insights into the
813 Pathogenesis and Treatment of Krabbe Disease. *Pediatr Endocrinol Rev.* 2016;13 Suppl
814 1:689-96.

815 45. Brady RO, Kanfer J, and Shapiro D. The Metabolism of Glucocerebrosides. I. Purification
816 and Properties of a Glucocerebroside-Cleaving Enzyme from Spleen Tissue. *J Biol Chem.*
817 1965;240:39-43.
818 46. Senkevich K, Zorca CE, Dworkind A, Rudakou U, Somerville E, Yu E, et al. GALC variants
819 affect galactosylceramidase enzymatic activity and risk of Parkinson's disease. *Brain.*
820 2023;146(5):1859-72.
821 47. Zhang X, Wu H, Tang B, and Guo J. Clinical, mechanistic, biomarker, and therapeutic
822 advances in GBA1-associated Parkinson's disease. *Transl Neurodegener.* 2024;13(1):48.
823 48. Liu GY, and Sabatini DM. mTOR at the nexus of nutrition, growth, ageing and disease.
824 *Nat Rev Mol Cell Biol.* 2020;21(4):183-203.
825 49. Nader WO, Brown KS, Boyle NR, Kaplelach AK, Abdelaziz SM, Davis SE, et al. TFEB
826 overexpression alleviates autophagy-lysosomal deficits caused by progranulin
827 insufficiency. *Sci Rep.* 2025;15(1):26217.
828 50. Chang MC, Srinivasan K, Friedman BA, Suto E, Modrusan Z, Lee WP, et al. Progranulin
829 deficiency causes impairment of autophagy and TDP-43 accumulation. *J Exp Med.*
830 2017;214(9):2611-28.
831 51. Shoshan-Barmatz V, De Pinto V, Zweckstetter M, Raviv Z, Keinan N, and Arbel N. VDAC,
832 a multi-functional mitochondrial protein regulating cell life and death. *Mol Aspects Med.*
833 2010;31(3):227-85.
834 52. Humphries AD, Streimann IC, Stojanovski D, Johnston AJ, Yano M, Hoogenraad NJ, et al.
835 Dissection of the mitochondrial import and assembly pathway for human Tom40. *J Biol*
836 *Chem.* 2005;280(12):11535-43.
837 53. Cardoso R, Lemos C, Oliveiros B, Almeida MR, Baldeiras I, Pereira CF, et al.
838 APOEvarepsilon4-TOMM40L Haplotype Increases the Risk of Mild Cognitive Impairment
839 Conversion to Alzheimer's Disease. *J Alzheimers Dis.* 2020;78(2):587-601.

840 54. Sen A, Kallabis S, Gaedke F, Jungst C, Boix J, Nuchel J, et al. Mitochondrial membrane
841 proteins and VPS35 orchestrate selective removal of mtDNA. *Nat Commun.*
842 2022;13(1):6704.
843 55. Rodriguez-Perinan G, de la Encarnacion A, Moreno F, Lopez de Munain A, Martinez A,
844 Martin-Requero A, et al. Progranulin Deficiency Induces Mitochondrial Dysfunction in
845 Frontotemporal Lobar Degeneration with TDP-43 Inclusions. *Antioxidants (Basel).*
846 2023;12(3).
847 56. Zhou D, Zhou M, Wang Z, Fu Y, Jia M, Wang X, et al. PGRN acts as a novel regulator of
848 mitochondrial homeostasis by facilitating mitophagy and mitochondrial biogenesis to
849 prevent podocyte injury in diabetic nephropathy. *Cell Death Dis.* 2019;10(7):524.
850 57. Geier EG, Bourdenx M, Storm NJ, Cochran JN, Sirkis DW, Hwang JH, et al. Rare variants
851 in the neuronal ceroid lipofuscinosis gene MFSD8 are candidate risk factors for
852 frontotemporal dementia. *Acta Neuropathol.* 2019;137(1):71-88.
853 58. Siintola E, Topcu M, Aula N, Lohi H, Minassian BA, Paterson AD, et al. The novel neuronal
854 ceroid lipofuscinosis gene MFSD8 encodes a putative lysosomal transporter. *Am J Hum*
855 *Genet.* 2007;81(1):136-46.
856 59. Zampieri S, Filocamo M, Pianta A, Lualdi S, Gort L, Coll MJ, et al. SMPD1 Mutation
857 Update: Database and Comprehensive Analysis of Published and Novel Variants. *Hum*
858 *Mutat.* 2016;37(2):139-47.
859 60. Elsea SH, Solyom A, Martin K, Harmatz P, Mitchell J, Lampe C, et al. ASAH1 pathogenic
860 variants associated with acid ceramidase deficiency: Farber disease and spinal muscular
861 atrophy with progressive myoclonic epilepsy. *Hum Mutat.* 2020;41(9):1469-87.
862 61. Wang X, Liang Y, Yang F, Shi Y, Shao R, Jing R, et al. Molecular mechanisms and targeted
863 therapy of progranulin in metabolic diseases. *Front Endocrinol (Lausanne).*
864 2025;16:1553794.

865 62. Singh S, Dransfeld UE, Ambaw YA, Lopez-Scarim J, Farese RV, Jr., and Walther TC.
866 PLD3 and PLD4 synthesize S,S-BMP, a key phospholipid enabling lipid degradation in
867 lysosomes. *Cell.* 2024;187(24):6820-34 e24.
868 63. Zhang T, Feng T, Wu K, Guo J, Nana AL, Yang G, et al. Progranulin deficiency results in
869 sex-dependent alterations in microglia in response to demyelination. *Acta Neuropathol.*
870 2023;146(1):97-119.
871 64. Hofmann SL, Atashband A, Cho SK, Das AK, Gupta P, and Lu JY. Neuronal ceroid
872 lipofuscinoses caused by defects in soluble lysosomal enzymes (CLN1 and CLN2). *Curr*
873 *Mol Med.* 2002;2(5):423-37.
874 65. Reifschneider A, Robinson S, van Lengerich B, Gnorich J, Logan T, Heindl S, et al. Loss
875 of TREM2 rescues hyperactivation of microglia, but not lysosomal deficits and
876 neurotoxicity in models of progranulin deficiency. *Embo J.* 2022;41(4):e109108.
877 66. Pesamaa I, Muller SA, Robinson S, Darcher A, Paquet D, Zetterberg H, et al. A microglial
878 activity state biomarker panel differentiates FTD-granulin and Alzheimer's disease patients
879 from controls. *Mol Neurodegener.* 2023;18(1):70.
880 67. Wang A, Chen C, Mei C, Liu S, Xiang C, Fang W, et al. Innate immune sensing of
881 lysosomal dysfunction drives multiple lysosomal storage disorders. *Nat Cell Biol.*
882 2024;26(2):219-34.
883 68. Chu TT, Tu X, Yang K, Wu J, Repa JJ, and Yan N. Tonic prime-boost of STING signalling
884 mediates Niemann-Pick disease type C. *Nature.* 2021;596(7873):570-5.
885 69. Hashimoto K, Jahan N, Miller ZA, and Huang EJ. Neuroimmune dysfunction in
886 frontotemporal dementia: Insights from progranulin and C9orf72 deficiency. *Curr Opin*
887 *Neurobiol.* 2022;76:102599.
888 70. Chowdhury SR, Parikh CN, Kaur AN, DeMarco KD, Giwa HK, Mishra AK, et al. PPT1 is a
889 negative regulator of STING signaling in cancer cells and its inhibition reactivates immune
890 surveillance in cold tumors. *Proc Natl Acad Sci U S A.* 2025;122(39):e2514948122.

891 71. Ramanjulu JM, Pesiridis GS, Yang J, Concha N, Singhaus R, Zhang SY, et al. Design of
892 amidobenzimidazole STING receptor agonists with systemic activity. *Nature.*
893 2018;564(7736):439-43.
894 72. Xu Y, and Wan W. Lysosomal control of the cGAS-STING signaling. *Trends Cell Biol.*
895 2024;34(8):622-5.
896 73. Hasan S, Fernandopulle MS, Humble SW, Frankenfield AM, Li H, Prestil R, et al. Multi-
897 modal Proteomic Characterization of Lysosomal Function and Proteostasis in Progranulin-
898 Deficient Neurons. *bioRxiv.* 2023.
899 74. Zhou X, Paushter DH, Pagan MD, Kim D, Nunez Santos M, Lieberman RL, et al.
900 Progranulin deficiency leads to reduced glucocerebrosidase activity. *PLoS One.*
901 2019;14(7):e0212382.
902 75. Boyle NR, Fox SN, Tadepalli AS, Seyfried NT, Kukar T, Ramos EM, et al. Reduction of
903 sphingomyelinase activity associated with progranulin deficiency and frontotemporal
904 dementia. *Neurobiol Dis.* 2025;213:107024.
905 76. Yang C, Du H, Lee GB, Uematsu M, He W, Dore E, et al. sPLA2-IIA modifies progranulin
906 deficiency phenotypes in mouse models. *Mol Neurodegener.* 2025;20(1):72.
907 77. Bajaj L, Sharma J, di Ronza A, Zhang P, Eblimit A, Pal R, et al. A CLN6-CLN8 complex
908 recruits lysosomal enzymes at the ER for Golgi transfer. *J Clin Invest.* 2020;130(8):4118-
909 32.
910 78. Devireddy S, and Ferguson SM. Efficient progranulin exit from the ER requires its
911 interaction with prosaposin, a Surf4 cargo. *J Cell Biol.* 2022;221(2).
912 79. Filippini F, Devireddy S, and Ferguson SM. LRP10 promotes trafficking of progranulin and
913 prosaposin to lysosomes. *bioRxiv.* 2025:2025.05.02.651888.
914 80. Udayar V, Chen Y, Sidransky E, and Jagasia R. Lysosomal dysfunction in
915 neurodegeneration: emerging concepts and methods. *Trends Neurosci.* 2022;45(3):184-
916 99.

917 81. Gomez-Sintes R, Ledesma MD, and Boya P. Lysosomal cell death mechanisms in aging.
918 *Ageing Res Rev.* 2016;32:150-68.
919 82. Sevigny J, Uspenskaya O, Heckman LD, Wong LC, Hatch DA, Tewari A, et al. Progranulin
920 AAV gene therapy for frontotemporal dementia: translational studies and phase 1/2 trial
921 interim results. *Nat Med.* 2024;30(5):1406-15.
922 83. Kurnellas M, Mitra A, Schwabe T, Paul R, Arrant AE, Roberson ED, et al. Latozinemab, a
923 novel progranulin-elevating therapy for frontotemporal dementia. *J Transl Med.*
924 2023;21(1):387.
925 84. Rosenthal ZC, Fass DM, Payne NC, She A, Patnaik D, Hennig KM, et al. Epigenetic
926 modulation through BET bromodomain inhibitors as a novel therapeutic strategy for
927 progranulin-deficient frontotemporal dementia. *Sci Rep.* 2024;14(1):9064.
928 85. Root J, Mendsaikhan A, Taylor G, Merino P, Nandy S, Wang M, et al. Granulins rescue
929 inflammation, lysosome dysfunction, lipofuscin, and neuropathology in a mouse model of
930 progranulin deficiency. *Cell Rep.* 2024;43(12):114985.
931 86. Selkoe DJ, and Hardy J. The amyloid hypothesis of Alzheimer's disease at 25 years.
932 *EMBO Mol Med.* 2016;8(6):595-608.
933 87. Morris HR, Spillantini MG, Sue CM, and Williams-Gray CH. The pathogenesis of
934 Parkinson's disease. *Lancet.* 2024;403(10423):293-304.
935 88. Benussi A, Alberici A, Samra K, Russell LL, Greaves CV, Bocchetta M, et al. Conceptual
936 framework for the definition of preclinical and prodromal frontotemporal dementia.
937 *Alzheimers Dement.* 2022;18(7):1408-23.
938 89. Frew J, and Nygaard HB. Neuropathological and behavioral characterization of aged Grn
939 R493X progranulin-deficient frontotemporal dementia knockin mice. *Acta Neuropathol*
940 *Commun.* 2021;9(1):57.

941 90. Phipson B, Lee S, Majewski IJ, Alexander WS, and Smyth GK. Robust Hyperparameter
942 Estimation Protects against Hypervariable Genes and Improves Power to Detect
943 Differential Expression. *Ann Appl Stat.* 2016;10(2):946-63.
944 91. Ritchie ME, Phipson B, Wu D, Hu Y, Law CW, Shi W, et al. limma powers differential
945 expression analyses for RNA-sequencing and microarray studies. *Nucleic Acids Res.*
946 2015;43(7):e47.
947 92. Ge SX, Jung D, and Yao R. ShinyGO: a graphical gene-set enrichment tool for animals
948 and plants. *Bioinformatics.* 2020;36(8):2628-9.

949

950

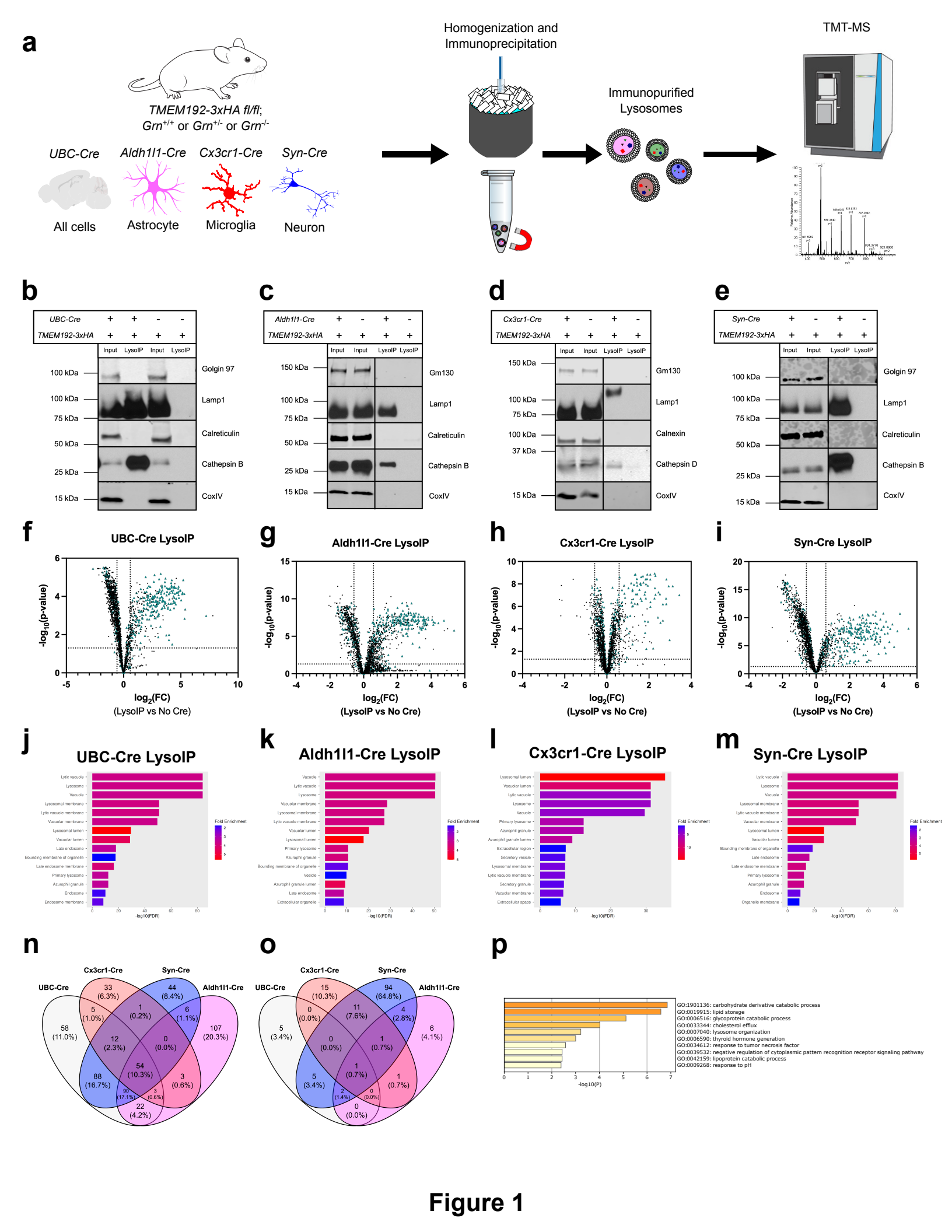
a
TMEM192-3xHA fl/fl;
Grn+/+ or Grn+/- or Grn-/-
UBC-Cre
Aldh1l1-Cre
Cx3cr1-Cre
Syn-Cre
All cells
Astrocyte
Microglia
Neuron
Homogenization and Immunoprecipitation
Immunopurified Lysosomes
TMT-MS
b
UBC-Cre
TMEM192-3xHA
Input LysoIP Input LysoIP
100 kDa Golgin 97
100 kDa Lamp1
75 kDa Calreticulin
50 kDa Cathepsin B
25 kDa CoxIV
15 kDa
c
Aldh1l1-Cre
TMEM192-3xHA
Input Input LysoIP LysoIP
150 kDa Gm130
100 kDa Lamp1
75 kDa Calreticulin
50 kDa Cathepsin B
25 kDa CoxIV
15 kDa
d
Cx3cr1-Cre
TMEM192-3xHA
Input Input LysoIP LysoIP
150 kDa Gm130
100 kDa Lamp1
75 kDa
100 kDa Calnexin
37 kDa Cathepsin D
15 kDa CoxIV
e
Syn-Cre
TMEM192-3xHA
Input Input LysoIP LysoIP
100 kDa Golgin 97
100 kDa Lamp1
75 kDa Calreticulin
50 kDa Cathepsin B
25 kDa CoxIV
15 kDa
f
UBC-Cre LysoIP
-log10(p-value)
log2(FC)
(LysoIP vs No Cre)
g
Aldh1l1-Cre LysoIP
-log10(p-value)
log2(FC)
(LysoIP vs No Cre)
h
Cx3cr1-Cre LysoIP
-log10(p-value)
log2(FC)
(LysoIP vs No Cre)
i
Syn-Cre LysoIP
-log10(p-value)
log2(FC)
(LysoIP vs No Cre)
j
UBC-Cre LysoIP
Lytic vacuole
Lysosome
Vacuole
Lysosomal membrane
Lytic vacuole membrane
Vacuolar membrane
Lysosomal lumen
Vacuolar lumen
Late endosome
Bounding membrane of organelle
Late endosome membrane
Primary lysosome
Azurophil granule
Endosome
Endosome membrane
Fold Enrichment
-log10(FDR)
k
Aldh1l1-Cre LysoIP
Vacuole
Lytic vacuole
Lysosome
Vacuolar membrane
Lysosomal membrane
Lytic vacuole membrane
Vacuolar lumen
Lysosomal lumen
Primary lysosome
Azurophil granule
Bounding membrane of organelle
Vesicle
Azurophil granule lumen
Late endosome
Extracellular organelle
Fold Enrichment
-log10(FDR)
l
Cx3cr1-Cre LysoIP
Lysosomal lumen
Vacuolar lumen
Lytic vacuole
Lysosome
Vacuole
Primary lysosome
Azurophil granule
Azurophil granule lumen
Extracellular region
Secretory vesicle
Lysosomal membrane
Lytic vacuole membrane
Secretory granule
Vacuolar membrane
Extracellular space
Fold Enrichment
-log10(FDR)
m
Syn-Cre LysoIP
Lytic vacuole
Lysosome
Vacuole
Lysosomal membrane
Lytic vacuole membrane
Vacuolar membrane
Lysosomal lumen
Vacuolar lumen
Bounding membrane of organelle
Late endosome
Late endosome membrane
Primary lysosome
Azurophil granule
Endosome
Organelle membrane
Fold Enrichment
-log10(FDR)
n
UBC-Cre
Cx3cr1-Cre
Syn-Cre
Aldh1l1-Cre
58 (11.0%)
33 (6.3%)
44 (8.4%)
107 (20.3%)
5 (1.0%)
1 (0.2%)
6 (1.1%)
12 (2.3%)
0 (0.0%)
54 (10.3%)
88 (16.7%)
3 (0.6%)
90 (17.1%)
3 (0.6%)
22 (4.2%)
o
UBC-Cre
Cx3cr1-Cre
Syn-Cre
Aldh1l1-Cre
5 (3.4%)
15 (10.3%)
94 (64.8%)
6 (4.1%)
0 (0.0%)
11 (7.6%)
4 (2.8%)
0 (0.0%)
1 (0.7%)
1 (0.7%)
5 (3.4%)
2 (1.4%)
0 (0.0%)
1 (0.7%)
0 (0.0%)
p
GO:1901136: carbohydrate derivative catabolic process
GO:0019915: lipid storage
GO:0006516: glycoprotein catabolic process
GO:0033344: cholesterol efflux
GO:0007040: lysosome organization
GO:0006590: thyroid hormone generation
GO:0034612: response to tumor necrosis factor
GO:0039532: negative regulation of cytoplasmic pattern recognition receptor signaling pathway
GO:0042159: lipoprotein catabolic process
GO:0009268: response to pH
-log10(P)

Figure 1

951 **Figure 1: *In vivo* LysoIP isolates cell-type-specific lysosomes from progranulin deficient**
952 **mice. a** Experimental design for cell-type-specific lysosomal isolation from progranulin deficient
953 mice followed by TMT-MS. **b-e** Western blot verification of *in vivo* LysoIP from all brain cells (*Ubc-*
954 *Cre*, **b**), microglia (*Cx3cr1-Cre*, **c**), astrocytes (*Aldh1l1-Cre*, **d**), and neurons (*Syn-Cre*, **e**). **f-i**
955 Volcano plots comparing LysoIP samples to no *Cre* controls (adjusted p-value < 0.05, one-sample
956 t-test followed by Benjamini-Hochberg correction). Known lysosomal proteins are marked as blue
957 triangles. **j-m** Gene ontology analysis of LysoIP samples from four separate *Cre* lines after
958 processing of raw TMT-MS peak intensities. **n** Venn diagram that demonstrates overlap of all
959 brain-derived, lysosomal proteins found in four separate *Cre* lines. **o** Venn diagram that
960 demonstrates overlap of significantly altered brain-derived, lysosomal proteins (*Grn* WT vs *Grn*
961 KO, adjusted p-value < 0.05) in four separate *Cre* lines. **p** Gene ontology analysis of significantly
962 altered, brain-derived lysosomal proteins found in all four *Cre* lines (*Grn* WT vs *Grn* KO, adjusted
963 p-value < 0.05).

964

965

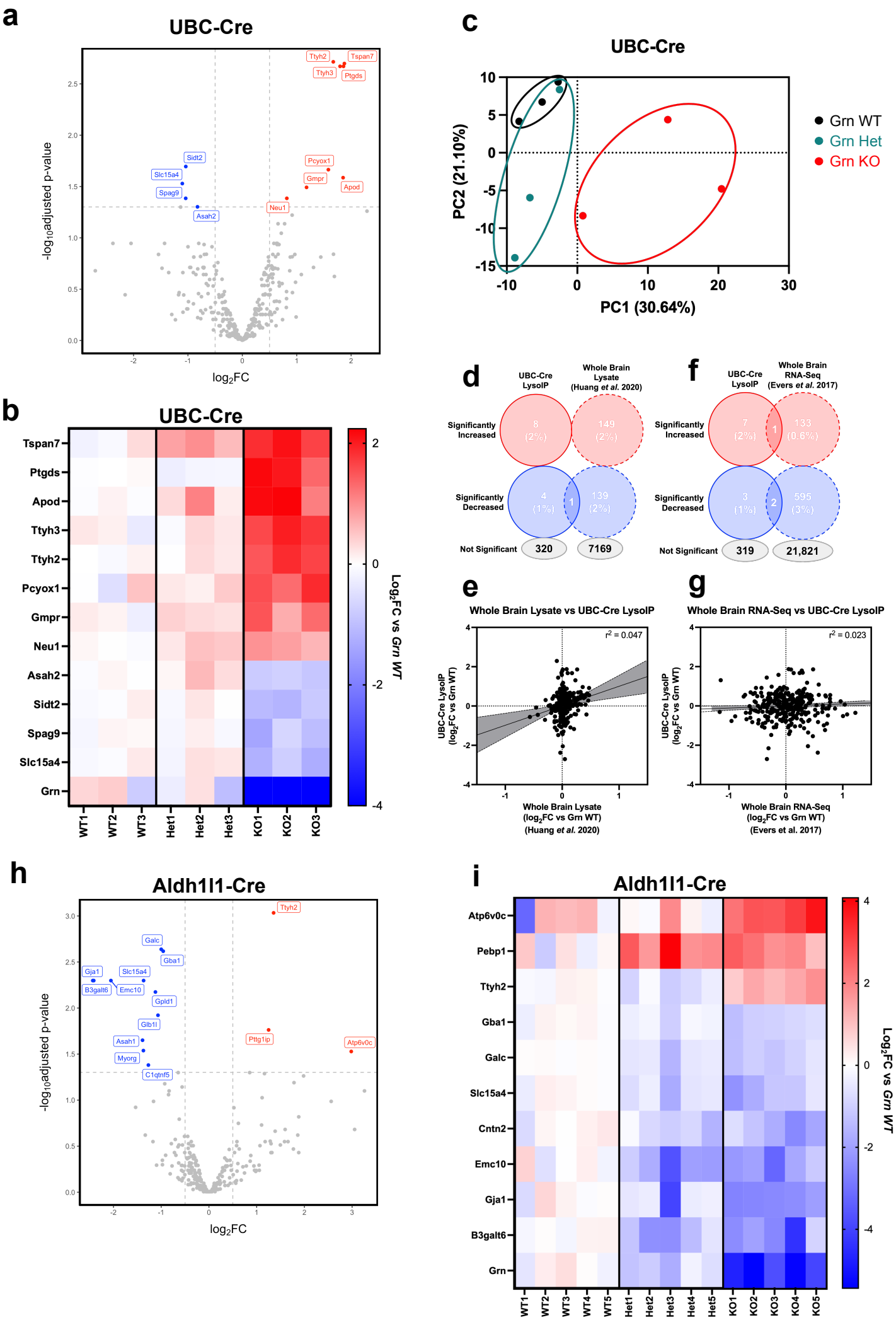
a
UBC-Cre
Ttyh2
Tspan7
Ttyh3
Ptgds
Sidt2
Slc15a4
Spag9
Asah2
Pcyox1
Gmpr
Apod
Neu1
-log10adjusted p-value
log2FC
b
UBC-Cre
Tspan7
Ptgds
Apod
Ttyh3
Ttyh2
Pcyox1
Gmpr
Neu1
Asah2
Sidt2
Spag9
Slc15a4
Grn
WT1
WT2
WT3
Het1
Het2
Het3
KO1
KO2
KO3
Log2FC vs Grn WT
c
UBC-Cre
PC2 (21.10%)
PC1 (30.64%)
Grn WT
Grn Het
Grn KO
d
UBC-Cre LysoIP
Whole Brain Lysate (Huang et al. 2020)
Significantly Increased
Significantly Decreased
Not Significant
8 (2%)
149 (2%)
4 (1%)
1
139 (2%)
320
7169
f
UBC-Cre LysoIP
Whole Brain RNA-Seq (Evers et al. 2017)
Significantly Increased
Significantly Decreased
Not Significant
7 (2%)
1
133 (0.6%)
3 (1%)
2
595 (3%)
319
21,821
e
Whole Brain Lysate vs UBC-Cre LysoIP
r2 = 0.047
UBC-Cre LysoIP (log2FC vs Grn WT)
Whole Brain Lysate (log2FC vs Grn WT) (Huang et al. 2020)
g
Whole Brain RNA-Seq vs UBC-Cre LysoIP
r2 = 0.023
UBC-Cre LysoIP (log2FC vs Grn WT)
Whole Brain RNA-Seq (log2FC vs Grn WT) (Evers et al. 2017)
h
Aldh1l1-Cre
Ttyh2
Galc
Gba1
Gja1
Slc15a4
B3galt6
Emc10
Gpld1
Glb1l
Asah1
Myorg
C1qtnf5
Pttg1ip
Atp6v0c
-log10adjusted p-value
log2FC
i
Aldh1l1-Cre
Atp6v0c
Pebp1
Ttyh2
Gba1
Galc
Slc15a4
Cntn2
Emc10
Gja1
B3galt6
Grn
WT1
WT2
WT3
WT4
WT5
Het1
Het2
Het3
Het4
Het5
KO1
KO2
KO3
KO4
KO5
Log2FC vs Grn WT

Figure 2

966 **Figure 2. *In vivo* LysoIP analysis of 3-month-old *Ubc-Cre* mouse brains demonstrates post-**
967 **translational alterations in key lysosomal proteins. a** Volcano plot demonstrating significantly
968 altered proteins (*Grn* WT vs *Grn* KO adjusted p-value < 0.05) from whole-brain LysoIP TMT-MS
969 samples (n = 3 *Grn* WT, n = 3 *Grn* Het, n = 3 *Grn* KO). **b** Principal component analysis comparing
970 $\log_2$FC values between *Grn* WT, *Grn* Het, and *Grn* KO brain-derived, lysosomal proteins in *Ubc-*
971 *Cre* mice. **c** Heatmap demonstrating $\log_2$FC values for significantly altered, brain-derived
972 lysosomal proteins found in brain-derived *Ubc-Cre* LysoIP TMT-MS samples (*Grn* WT vs *Grn* KO,
973 adjusted p-value < 0.05). **d** Venn diagram of the overlap of significantly altered proteins (*Grn* WT
974 vs *Grn* KO, adjusted p-value < 0.05) between brain-derived *Ubc-Cre* LysoIP and previously
975 published whole brain, whole cell lysate TMT-MS experiments. **e** Venn diagram of the overlap of
976 significantly altered proteins/transcripts (*Grn* WT vs *Grn* KO, adjusted p-value/q-value < 0.05)
977 between brain-derived *Ubc-Cre* LysoIP TMT-MS samples and previously published whole brain
978 RNA-Seq data. **f** Comparison of all $\log_2$FC values (*Grn* WT vs *Grn* KO) for proteins found in both
979 brain-derived *Ubc-Cre* LysoIP TMT-MS samples and previously published whole brain TMT-MS
980 datasets **g** Comparison of all $\log_2$FC values (*Grn* WT vs *Grn* KO) for proteins/transcripts found in
981 both brain-derived *Ubc-Cre* LysoIP TMT-MS samples and previously published whole brain RNA-
982 Seq datasets. **h** Volcano plot demonstrating significantly altered proteins (*Grn* WT vs *Grn* KO
983 adjusted p-value < 0.05) from whole-brain *Aldh1l1-Cre* LysoIP TMT-MS samples (n = 5 *Grn* WT,
984 n = 5 *Grn* Het, n = 5 *Grn* KO). **i** Heatmap demonstrating $\log_2$FC values for significantly altered,
985 brain-derived lysosomal proteins found in brain-derived *Aldh1l1-Cre* LysoIP TMT-MS samples
986 (*Grn* WT vs *Grn* KO, adjusted p-value < 0.05).

987

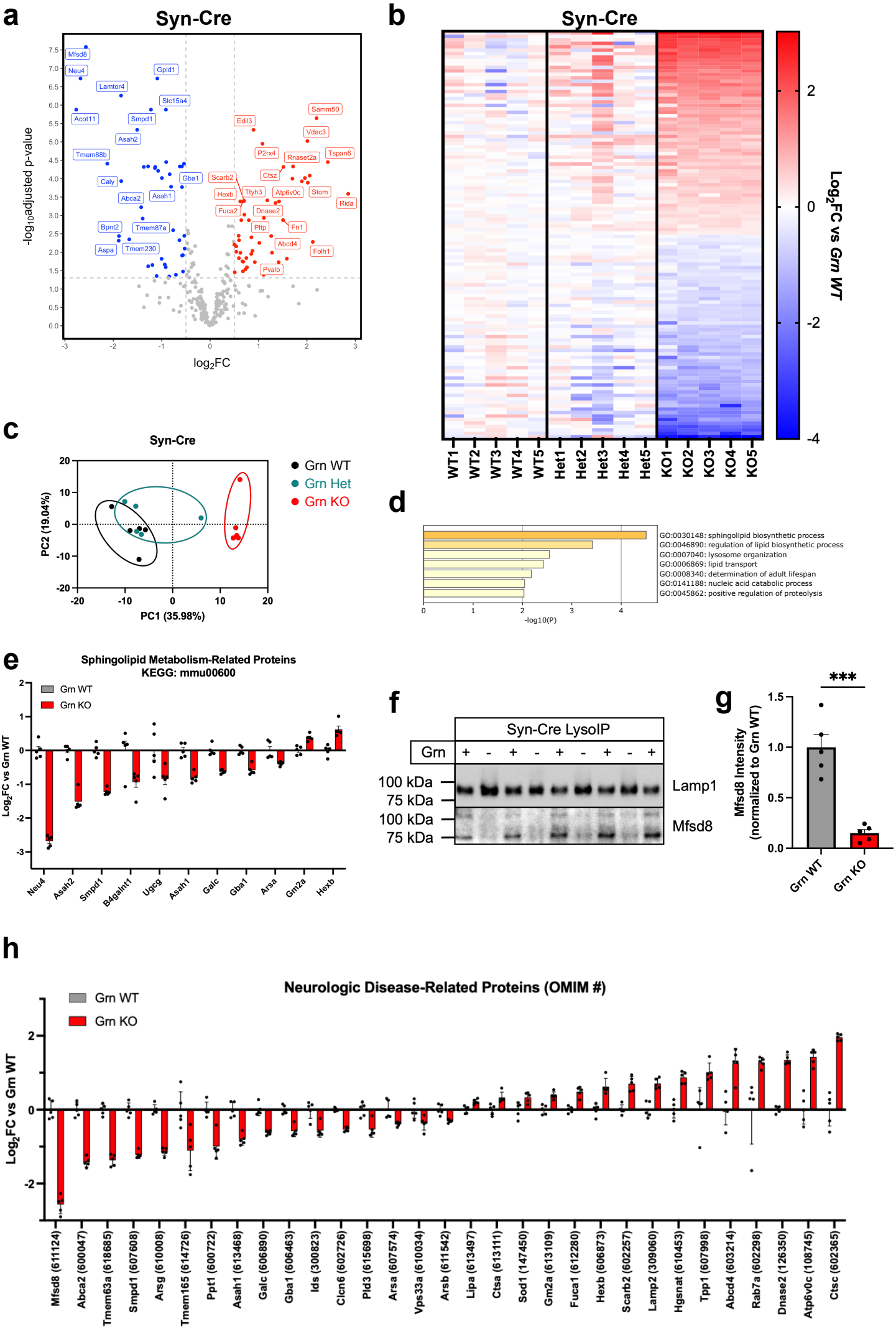
a
Syn-Cre
-log10adjusted p-value
log2FC
Mfsd8
Neu4
Gpld1
Lamtor4
Slc15a4
Acot11
Smpd1
Asah2
Tmem88b
Caly
Gba1
Abca2
Asah1
Bpnt2
Tmem87a
Aspa
Tmem230
Samm50
Edil3
Vdac3
P2rx4
Rnaset2a
Tspan6
Ctsz
Scarb2
Hexb
Ttyh3
Atp6v0c
Stom
Rida
Fuca2
Dnase2
Pltp
Fn1
Abcd4
Folh1
Pvalb
b
Syn-Cre
Log2FC vs Grn WT
WT1
WT2
WT3
WT4
WT5
Het1
Het2
Het3
Het4
Het5
KO1
KO2
KO3
KO4
KO5
c
Syn-Cre
Grn WT
Grn Het
Grn KO
PC2 (19.04%)
PC1 (35.98%)
d
GO:0030148: sphingolipid biosynthetic process
GO:0046890: regulation of lipid biosynthetic process
GO:0007040: lysosome organization
GO:0006869: lipid transport
GO:0008340: determination of adult lifespan
GO:0141188: nucleic acid catabolic process
GO:0045862: positive regulation of proteolysis
-log10(P)
e
Sphingolipid Metabolism-Related Proteins
KEGG: mmu00600
Grn WT
Grn KO
Log2FC vs Grn WT
Neu4
Asah2
Smpd1
B4galnt1
Ugcg
Asah1
Galc
Gba1
Arsa
Gm2a
Hexb
f
Syn-Cre LysoIP
Grn
100 kDa
75 kDa
100 kDa
75 kDa
Lamp1
Mfsd8
g
***
Mfsd8 Intensity
(normalized to Grn WT)
Grn WT
Grn KO
h
Neurologic Disease-Related Proteins (OMIM #)
Grn WT
Grn KO
Log2FC vs Grn WT
Mfsd8 (611124)
Abca2 (600047)
Tmem63a (618685)
Smpd1 (607608)
Arsg (610008)
Tmem165 (614726)
Ppt1 (600722)
Asah1 (613468)
Galc (606890)
Gba1 (606463)
Ids (300823)
Clcn6 (602726)
Pld3 (615698)
Arsa (607574)
Vps33a (610034)
Arsb (611542)
Lipa (613497)
Ctsa (613111)
Sod1 (147450)
Gm2a (613109)
Fuca1 (612280)
Hexb (606873)
Scarb2 (602257)
Lamp2 (309060)
Hgsnat (610453)
Tpp1 (607998)
Abcd4 (603214)
Rab7a (602298)
Dnase2 (126350)
Atp6v0c (108745)
Ctsc (602365)

Figure 3

988 **Figure 3. *In vivo* LysoIP analysis of 3-month-old *Syn-Cre* mouse brains demonstrates**
989 **aberrations in disease-relevant lysosomal proteins in progranulin-deficient neurons. a**
990 Volcano plot demonstrating significantly altered proteins (*Grn* WT vs *Grn* KO adjusted p-value <
991 0.05) from neuronal LysoIP TMT-MS samples (n = 5 *Grn* WT, n = 5 *Grn* Het, n = 5 *Grn* KO). **b**
992 Heatmap demonstrating $\log_2$FC values for significantly altered neuronal LysoIP samples (*Grn* WT
993 vs *Grn* KO, adjusted p-value < 0.05). **c** Principal component analysis comparing $\log_2$FC values in
994 neuronal lysosomal proteins between *Grn* WT, *Grn* Het, and *Grn* KO mice. **d** Gene ontology
995 analysis of significantly altered neuronal lysosomal proteins (*Grn* WT vs *Grn* KO, adjusted p-value
996 < 0.05). **e** Significantly altered neuronal lysosomal proteins (*Grn* WT vs *Grn* KO, adjusted p-value
997 < 0.05) which are associated with sphingolipid metabolic processes based on gene ontology
998 analysis. **f-g** Western blot (**f**) and densitometry analysis (**g**) of Mfsd8 in neuronal lysosomes (n =
999 5 *Grn* WT, n = 4 *Grn* KO; ***p < 0.001, Students' t-test) **h** Significantly altered neuronal lysosomal
1000 proteins (*Grn* WT vs *Grn* KO, adjusted p-value < 0.05) whose mutations are associated with
1001 neurologic disease.

1002

1003

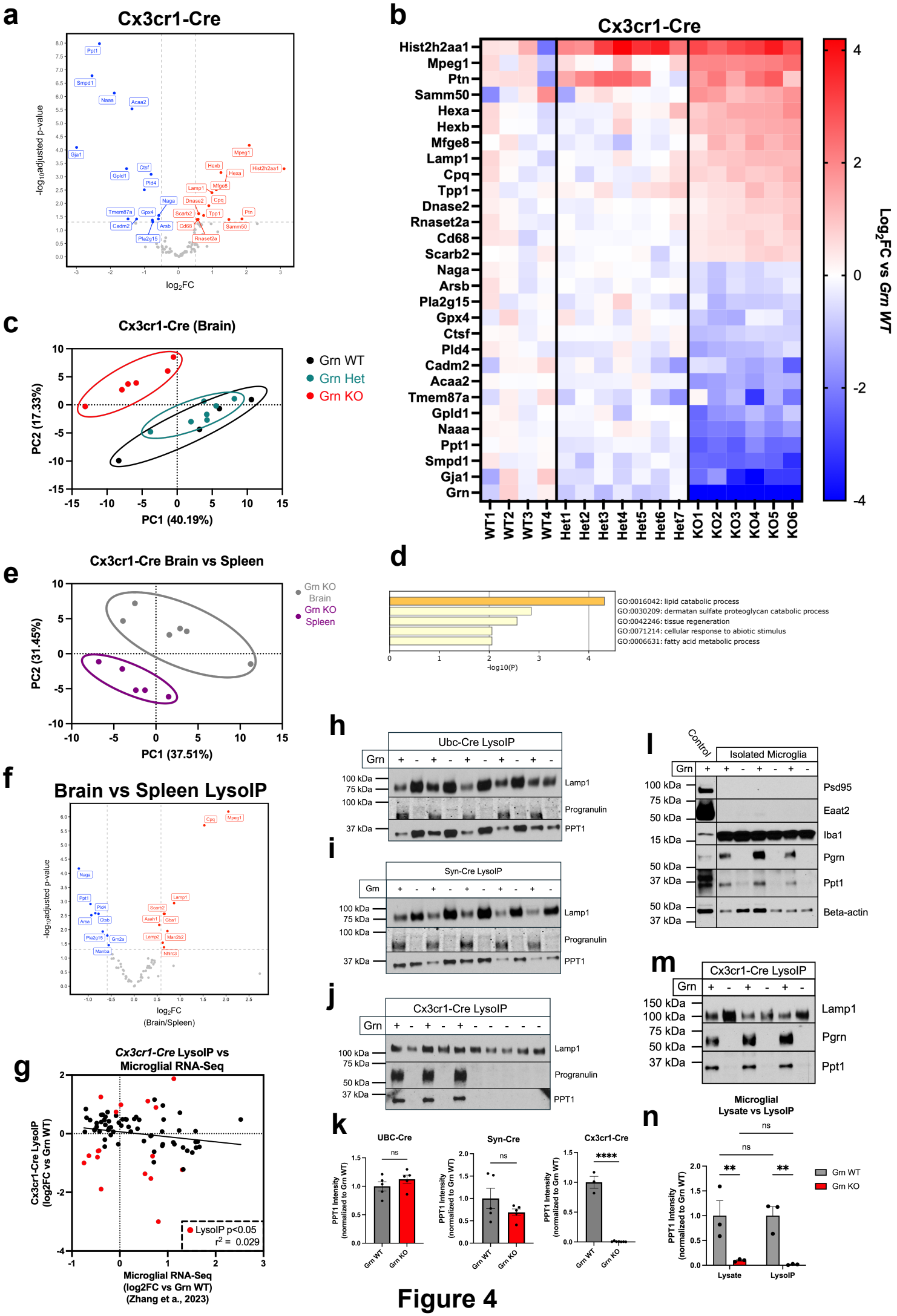
a
Cx3cr1-Cre
-log10adjusted p-value
log2FC
b
Cx3cr1-Cre
Hist2h2aa1
Mpeg1
Ptn
Samm50
Hexa
Hexb
Mfge8
Lamp1
Cpq
Tpp1
Dnase2
Rnaset2a
Cd68
Scarb2
Naga
Arsb
Pla2g15
Gpx4
Ctsf
Pld4
Cadm2
Acaa2
Tmem87a
Gpld1
Naaa
Ppt1
Smpd1
Gja1
Grn
WT1 WT2 WT3 WT4 Het1 Het2 Het3 Het4 Het5 Het6 Het7 KO1 KO2 KO3 KO4 KO5 KO6
Log2FC vs Grn WT
c
Cx3cr1-Cre (Brain)
PC2 (17.33%)
PC1 (40.19%)
Grn WT
Grn Het
Grn KO
d
GO:0016042: lipid catabolic process
GO:0030209: dermatan sulfate proteoglycan catabolic process
GO:0042246: tissue regeneration
GO:0071214: cellular response to abiotic stimulus
GO:0006631: fatty acid metabolic process
-log10(P)
e
Cx3cr1-Cre Brain vs Spleen
PC2 (31.45%)
PC1 (37.51%)
Grn KO Brain
Grn KO Spleen
f
Brain vs Spleen LysoIP
-log10adjusted p-value
log2FC
(Brain/Spleen)
g
Cx3cr1-Cre LysoIP vs Microglial RNA-Seq
Cx3cr1-Cre LysoIP (log2FC vs Grn WT)
Microglial RNA-Seq (log2FC vs Grn WT) (Zhang et a., 2023)
LysoIP p<0.05
r2 = 0.029
h
Ubc-Cre LysoIP
Grn
100 kDa
75 kDa
100 kDa
37 kDa
Lamp1
Progranulin
PPT1
i
Syn-Cre LysoIP
j
Cx3cr1-Cre LysoIP
150 kDa
50 kDa
l
Control
Isolated Microglia
Psd95
Eaat2
Iba1
Pgrn
Ppt1
Beta-actin
m
Cx3cr1-Cre LysoIP
k
UBC-Cre
Syn-Cre
Cx3cr1-Cre
PPT1 Intensity (normalized to Grn WT)
ns
****
Grn WT
Grn KO
n
Microglial Lysate vs LysoIP
Lysate
LysoIP
**

Figure 4

1004 **Figure 4. *In vivo* LysoIP analysis of 3-month-old *Cx3cr1-Cre* mouse brains demonstrates**
1005 **cell-specific loss of lysosomal storage disease-related protein in progranulin-deficient**
1006 **microglia. a** Volcano plot demonstrating significantly altered proteins (*Grn* WT vs *Grn* KO
1007 adjusted p-value < 0.05) from microglial LysoIP TMT-MS samples (n = 4 *Grn* WT, n = 7 *Grn* Het,
1008 n = 6 *Grn* KO). **b** Gene ontology analysis of significantly altered microglial lysosomal proteins (*Grn*
1009 WT vs *Grn* KO, adjusted p-value < 0.05). **c** Principal component analysis comparing $\log_2$FC
1010 values in microglial lysosomal proteins between *Grn* WT, *Grn* Het, and *Grn* KO mice. **d** Heatmap
1011 demonstrating $\log_2$FC values for significantly altered microglial LysoIP samples (*Grn* WT vs *Grn*
1012 KO, adjusted p-value < 0.05). **e** Principal component analysis comparing $\log_2$FC (*Grn* WT vs *Grn*
1013 KO) between brain- and spleen-derived *Cx3cr1-Cre* LysoIP samples. **f** Volcano plot
1014 demonstrating significantly altered proteins (brain vs spleen adjusted p-value < 0.05) from brain-
1015 and spleen-derived *Cx3cr1-Cre* LysoIP TMT-MS samples (n = 6 brain-derived, n = 6 spleen-
1016 derived). **g** Comparison of log2FC values (*Grn* WT vs *Grn* KO) between *Cx3cr1-Cre* LysoIP
1017 samples and microglial mRNA transcripts from a previously published RNA-Seq dataset. Red
1018 circles indicate proteins significantly altered in *Cx3cr1-Cre*+;*Grn* KO LysoIP samples. **h-j** Western
1019 blot analysis of Ppt1 in whole-brain (**h**) neuronal (**i**), and microglial (**j**) lysosomes derived from *Grn*
1020 WT and KO mouse brains. **k** Densitometry analysis of Ppt1 protein in whole-brain, neuronal, and
1021 microglial lysosomes derived from *Grn* WT and KO mouse brains. Values were standardized to
1022 Lamp1 and normalized to *Grn* WT (whole-brain: n = 5 3-month-old *Grn* WT and n = 5 3-month-
1023 old *Grn* KO; neuronal: n = 5 3-month-old *Grn* WT and n = 5 3-month-old *Grn* KO; microglia: n = 3
1024 6-month-old *Grn* WT and n = 7 6-month-old *Grn* KO; ****p < 0.0001, Students' t-test). **l-m** Western
1025 blot analysis of Ppt1 in microglial lysosomes (**l**) and whole microglia (**m**). Psd95, Eeat2, and Iba1
1026 act as neuronal, astrocyte, and microglial markers, respectively. **n** Densitometry analysis of Ppt1
1027 blots. Values were standardized to Lamp1 (**l**) or beta-actin (**m**) and normalized to *Grn* WT (n = 3
1028 9-12-month-old *Grn* WT and n = 3 9-12-month-old *Grn* KO; **p < 0.01, two-way ANOVA with
1029 Fisher's LSD test).

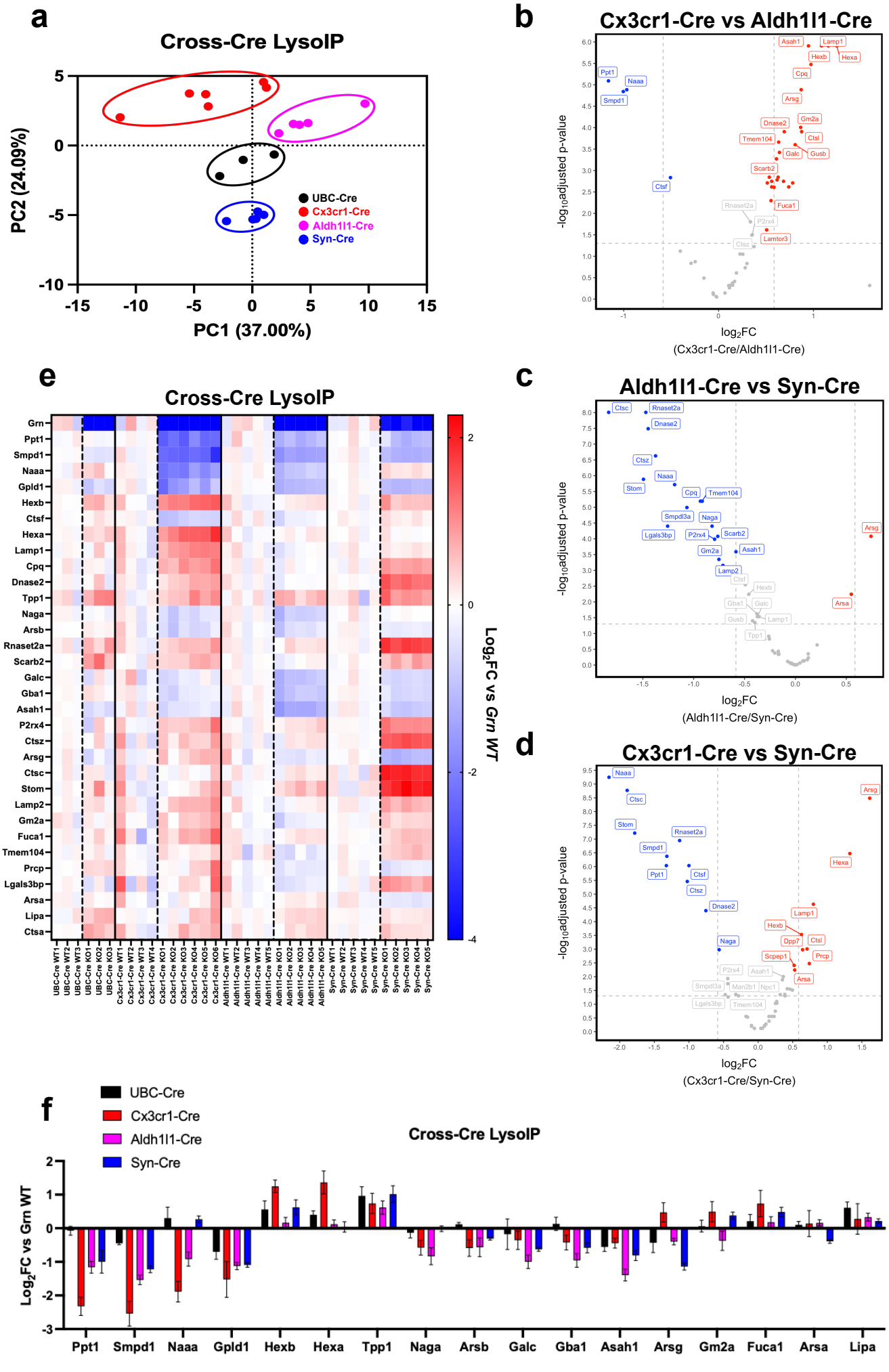
a
Cross-Cre LysoIP
PC2 (24.09%)
PC1 (37.00%)
UBC-Cre
Cx3cr1-Cre
Aldh1l1-Cre
Syn-Cre
b
Cx3cr1-Cre vs Aldh1l1-Cre
-log10adjusted p-value
log2FC
(Cx3cr1-Cre/Aldh1l1-Cre)
c
Aldh1l1-Cre vs Syn-Cre
-log10adjusted p-value
log2FC
(Aldh1l1-Cre/Syn-Cre)
d
Cx3cr1-Cre vs Syn-Cre
-log10adjusted p-value
log2FC
(Cx3cr1-Cre/Syn-Cre)
e
Cross-Cre LysoIP
Log2FC vs Grn WT
f
UBC-Cre
Cx3cr1-Cre
Aldh1l1-Cre
Syn-Cre
Cross-Cre LysoIP
Log2FC vs Grn WT
Ppt1
Smpd1
Naaa
Gpld1
Hexb
Hexa
Tpp1
Naga
Arsb
Galc
Gba1
Asah1
Arsg
Gm2a
Fuca1
Arsa
Lipa

Figure 5

1030 **Figure 5. *In vivo* LysoIP datasets demonstrate progranulin-dependent aberrations to the**
1031 **lysosomal proteome are unique across brain cell types. a** Principal component analysis of
1032 *Grn* KO LysoIP log_2FC values (*Grn* WT vs *Grn* KO) from four separate *Cre* lines. **b** Heatmap
1033 depicting log_2FC values (*Grn* WT vs *Grn* KO) of all proteins detected as significantly altered in
1034 *Grn* KO LysoIP samples (*Grn* WT vs *Grn* KO adjusted p-value < 0.05) in at least one *Cre* line. **c-**
1035 **e** Volcano plots comparing log_2FC values of significantly altered proteins (*Grn* WT vs *Grn* KO
1036 adjusted p-value < 0.05) between *Cx3cr1-Cre* and *Aldh1l1-Cre* (**c**), *Aldh1l1-Cre* and *Syn-Cre* (**d**),
1037 and *Cx3cr1-Cre* vs *Syn-Cre* (**e**) *Grn* KO LysoIP samples. **f** Bar plot comparing log_2FC values (*Grn*
1038 WT vs *Grn* KO) of key lysosomal proteins detected as significantly altered in *Grn* KO LysoIP
1039 samples (*Grn* WT vs *Grn* KO adjusted p-value < 0.05) in at least one *Cre* line.

1040

1041

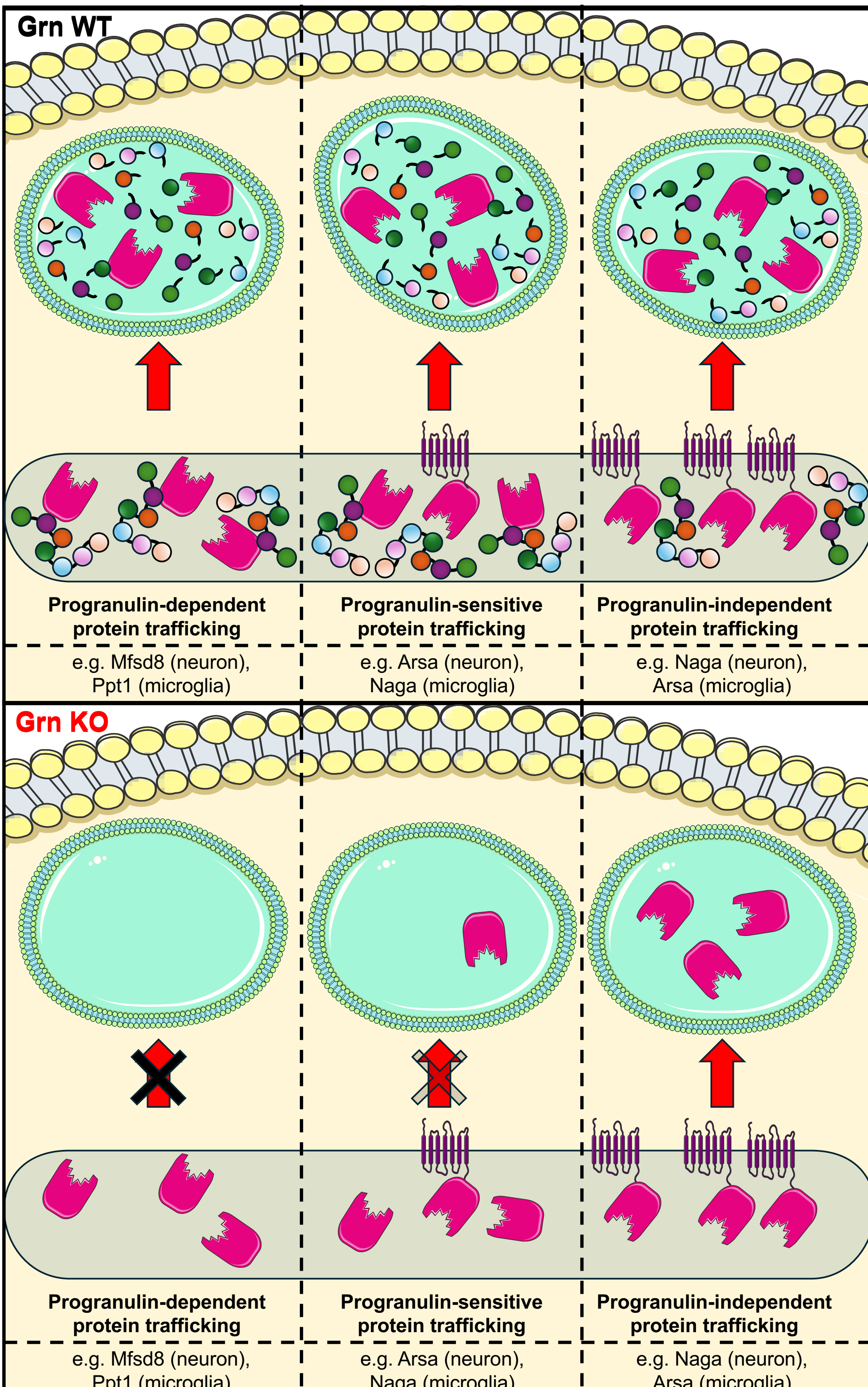
Grn WT
Progranulin-dependent protein trafficking
Progranulin-sensitive protein trafficking
Progranulin-independent protein trafficking
e.g. Mfsd8 (neuron), Ppt1 (microglia)
e.g. Arsa (neuron), Naga (microglia)
e.g. Naga (neuron), Arsa (microglia)
Grn KO
Progranulin-dependent protein trafficking
Progranulin-sensitive protein trafficking
Progranulin-independent protein trafficking
e.g. Mfsd8 (neuron), Ppt1 (microglia)
e.g. Arsa (neuron), Naga (microglia)
e.g. Naga (neuron), Arsa (microglia)

Figure 6

1042 **Figure 6. Hypothetical model of how progranulin deficiency potentially alters the**
1043 **lysosomal proteome in a cell-type specific way.** Hypothetical model depicting how in certain
1044 cell-types, lysosomal proteins may be fully dependent, partially dependent, or independent of
1045 progranulin for sorting to the lysosome. The variation between cell types may depend on yet
1046 unknown cell-type specific redundant proteins that, like progranulin, also sort lysosomal proteins
1047 to the lysosome. Some proteins, such as Mfsd8 in neurons or Ppt1 in microglia, are entirely or
1048 nearly entirely dependent upon progranulin for their lysosomal delivery (left panels). Other
1049 lysosomal proteins require progranulin for their efficient delivery, but can still complete their
1050 journey there, albeit at reduced overall efficiency (middle panels). For other proteins, sorting to
1051 the lysosome is undiminished even in the complete absence of progranulin (right panels).

1052

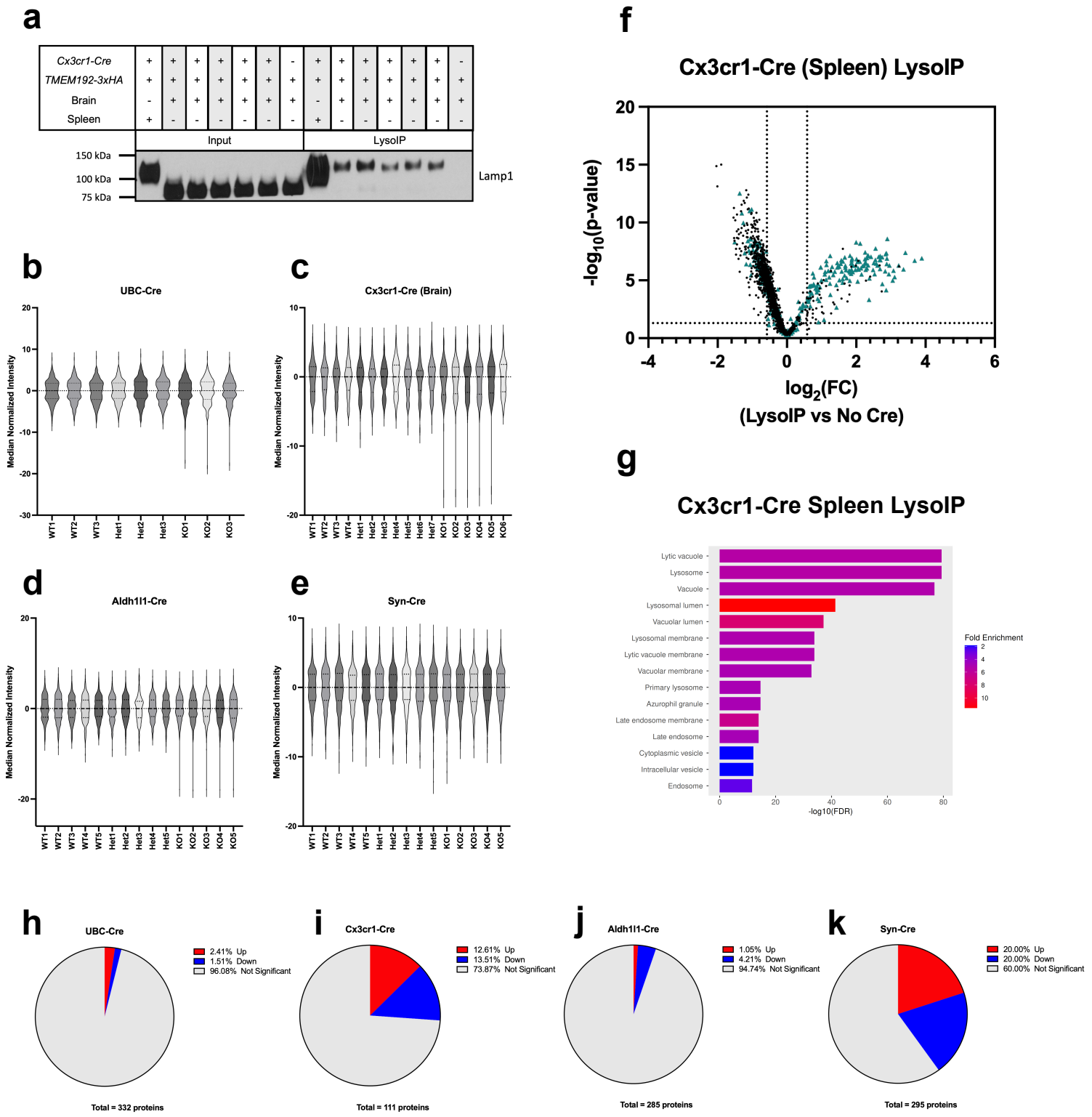

Supplemental Figure 1

1053 **Supplemental Figure 1. TMT-MS analysis of LysoIP samples demonstrates progranulin-**
1054 **dependent changes primarily in microglia and neurons. a-d** Violin plots of median-normalized
1055 TMT-MS intensity measurements from *Ubc-Cre* (**a**), *Cx3cr1-Cre* (**b**), *Aldh1l1-Cre* (**c**), and *Syn-*
1056 *Cre* (**d**) mice. Gm130 was used as a marker for Golgi apparatus, Lamp1 was used as a marker
1057 for lysosomal membrane, calnexin was used as a marker for ER, Cathepsin B was used as a
1058 marker for lysosomal lumen, and CoxIV was used as a marker for mitochondria. For *Cx3cr1-Cre*+
1059 samples, cathepsin D was used as a marker for lysosomal lumen due to these samples being
1060 imaged on Licor which was not compatible with our cathepsin B antibody. **e** Volcano plot
1061 comparing spleen-derived *Cx3cr1-Cre* LysoIP samples to no *Cre* controls (adjusted p-value <
1062 0.05, one-sample t-test followed by Benjamini-Hochberg correction). Known lysosomal proteins
1063 are marked as blue triangles. **f** Gene ontology analysis of spleen-derived *Cx3cr1-Cre* LysoIP
1064 samples after processing of raw TMT-MS peak intensities. **g** Lamp1 western blot of spleen- and
1065 brain-derived *Cx3cr1-Cre* whole lysate, LysoIP, and no *Cre* control samples. **h-k** Pie charts
1066 demonstrating percent of proteins significantly up- and down-regulated in whole-brain (**h**),
1067 microglial (**i**), astrocyte (**j**), and neuronal (**k**) lysosomes.

1068

1069

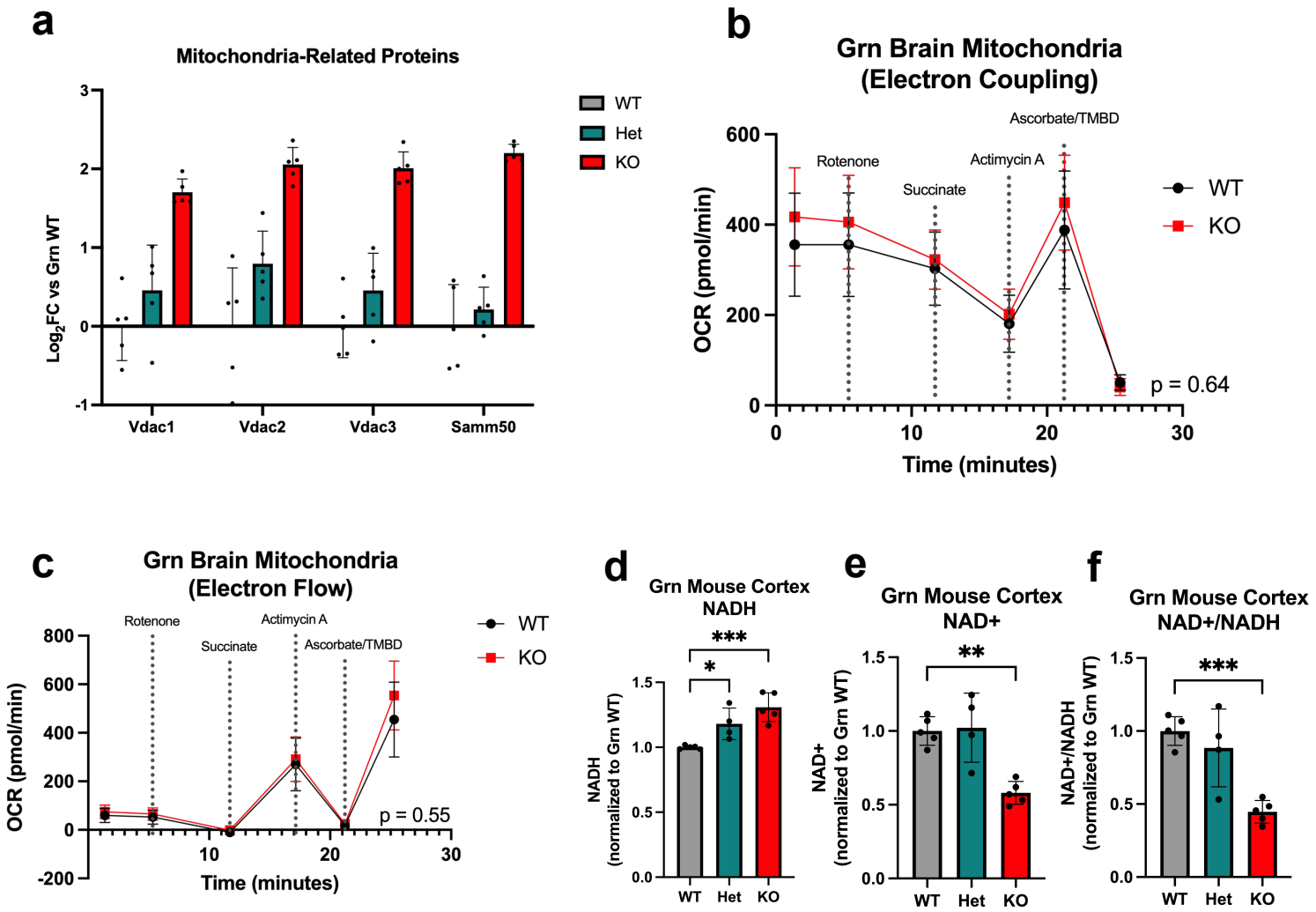

Supplemental Figure 2

1070 **Supplemental Figure 2. Progranulin deficiency leads to aberrant mitochondrial protein**
1071 **levels in neuronal lysosomes alongside energetic alterations. a** Log_2FC values of
1072 mitochondrial proteins significantly increased in *Grn* KO neuronal lysosomes compared to *Grn*
1073 WT (adjusted p-value < 0.05). **b-c** Seahorse analysis of electron flow (**b**) and electron coupling
1074 (**c**) of isolated mitochondria from 15-month-old *Grn* WT and *Grn* KO mouse brains (n = 3 *Grn* WT
1075 and n = 3 *Grn* KO; two-way ANOVA with multiple comparisons and Sidak correction). **d-f** Levels
1076 of NADH (**d**), NAD+ (**e**), and NAD+/NADH ratios (**f**) from 15-month-old *Grn* WT, *Grn* Het, and *Grn*
1077 KO mouse brains (n = 5 *Grn* WT, n = 4 *Grn* Het, n = 5 *Grn* KO; one-way ANOVA with multiple
1078 comparisons and Dunnett correction, *p < 0.05, **p < 0.01, ***p < 0.0001).

1079

1080

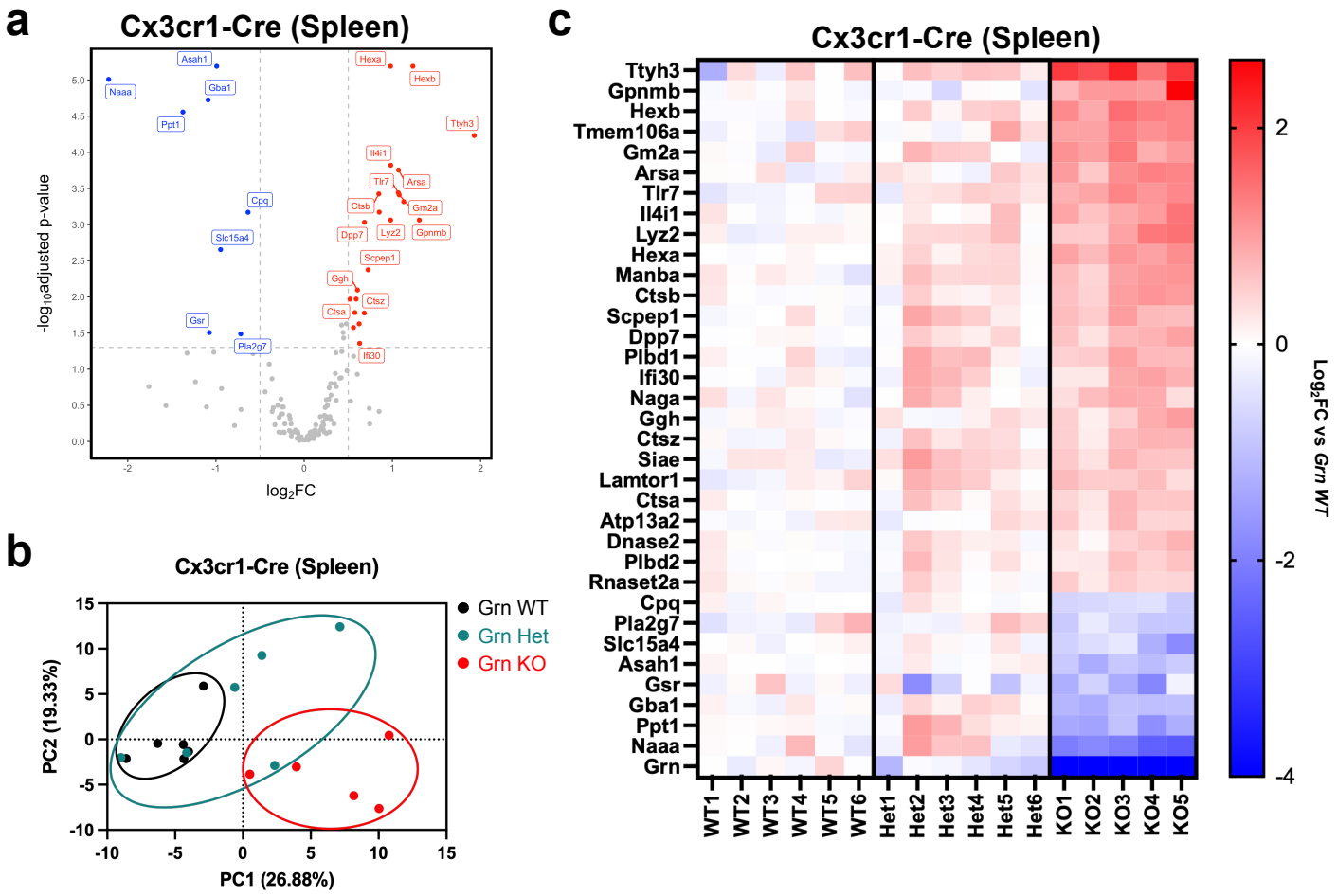

Supplemental Figure 3

1081 **Supplemental Figure 3. *In vivo* LysoIP analysis of 3-month-old *Cx3cr1-Cre* mouse spleens**
1082 **demonstrates progranulin-dependent changes in key lysosomal proteins. a** Volcano plot
1083 demonstrating significantly altered proteins (*Grn* WT vs *Grn* KO, adjusted p-value < 0.05) from
1084 splenic macrophage LysoIP TMT-MS samples (n = 6 *Grn* WT, n = 5 *Grn* Het, n = 5 *Grn* KO). **b**
1085 Principal component analysis comparing $\log_2$FC values in splenic macrophage lysosomal proteins
1086 between *Grn* WT, *Grn* Het, and *Grn* KO mice. **c** Venn diagram comparing significantly altered
1087 proteins (*Grn* WT vs *Grn* KO, adjusted p-values < 0.05) in splenic macrophage and microglial
1088 lysosomes.

1089

1090

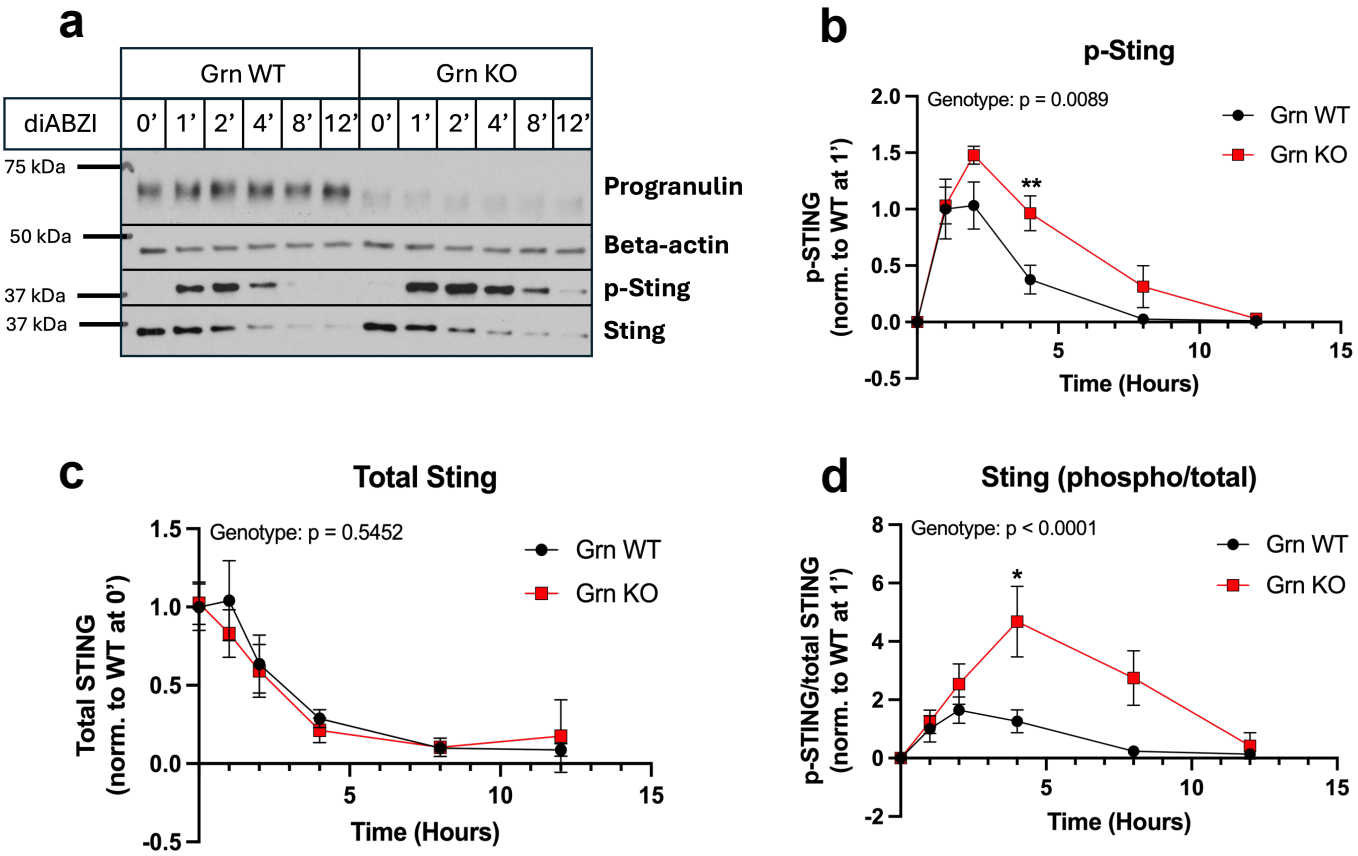

Supplemental Figure 4

1091 **Supplemental Figure 4. Progranulin deficiency leads to altered STING dynamics *in vitro*. a**
1092 Representative western blot of diABZI-mediated STING activation time course on *GRN* WT and
1093 *GRN* KO HeLa cells. Beta-actin is used as a loading control. **b-d** Quantification of p-STING (**b**),
1094 total STING (**c**), and phospho/total STING (**d**) of diABZI-mediated STING activation time course
1095 (n = 4 *GRN* WT, n = 4 *GRN* KO; two-way ANOVA with multiple comparisons and Sidak correction,
1096 *$p < 0.05$, **$p < 0.01$).

1097

1098

1099 **Table 1: List of endo-lysosomal disease related proteins significantly altered in**

1100 **progranulin-deficient neuronal lysosomes.**

Gene Name	OMIM#	Disease	Log_2FC (*Grn* KO/*Grn* WT)
Abca2	600047	Intellectual developmental disorder with poor growth and with or without seizures or ataxia	-1.422
Abcd4	603214	Methylmalonic aciduria and homocystinuria, cblJ type	1.2586
Arsa	607574	Metachromatic leukodystrophy	-0.3898
Arsb	611542	Mucopolysaccharidosis type VI (Maroteaux-Lamy)	-0.3096
Arsg	610008	Usher syndrome, type IV	-1.14
Asah1	613468	Farber lipogranulomatosis	-0.8072
Atp6v0c	108745	Epilepsy, early-onset, 3, with or without developmental delay	1.424
Clcn6	602726	Ceroid lipofuscinosis, neuronal, 15	-0.5394
Ctsa	613111	Galactosialidosis	0.3282
Ctsc	602365	Haim-Munk syndrome	1.958
Dnase2	126350	Autoinflammatory-pancytopenia syndrome	1.35
Fuca1	612280	Fucosidosis	0.4864
Galc	606890	Krabbe disease	-0.6264
Gba1	606463	Gaucher Disease	-0.5804
Gm2a	613109	GM2-gangliosidosis, AB variant	0.3804

Grn	138945	Ceroid lipofuscinosis, neuronal, 11	-4.226
Hexb	606873	Sandhoff disease, infantile, juvenile, and adult forms	0.6222
Hgsnat	610453	Mucopolysaccharidosis type IIIC (Sanfilippo C)	0.8754
Ids	300823	Mucopolysaccharidosis II	-0.5634
Lamp2	309060	Danon disease	0.7078
Lipa	613497	Cholesteryl ester storage disease	0.2158
Mfsd8	611124	Ceroid lipofuscinosis, neuronal, 7	-2.568
Pld3	615698	Spinocerebellar ataxia 46	-0.5342
Ppt1	600722	Ceroid lipofuscinosis, neuronal, 1	-0.9972
Rab7a	602298	Charcot-Marie-Tooth disease, type 2B	1.28
Scarb2	602257	Epilepsy, progressive myoclonic 4, with or without renal failure	0.7028
Smpd1	607608	Niemann-Pick disease, type A/B	-1.222
Sod1	147450	Parkinson's Disease	0.3346
Tmem165	614726	Congenital disorder of glycosylation, type IIk	-1.1058
Tmem63a	618685	Leukodystrophy, hypomyelinating, 19, transient infantile	-1.368
Tpp1	607998	Ceroid lipofuscinosis, neuronal, 2	1.0158
Vps33a	610034	Mucopolysaccharidosis-plus syndrome	-0.371

1103 **Supplemental Tables**

1104 **Supplemental Table 1:** Gene ontology analysis of LysoIP proteins significantly altered (*Grn* WT
1105 vs *Grn* KO) in at least one Cre line

1106 **Supplemental Table 2:** Log_2FC and p-values for TMT-MS data for individual mouse LysoIP data
1107 from all *Ubc-Cre+* lines compared to one another

1108 **Supplemental Table 3:** Log_2FC and p-values for TMT-MS data for individual mouse LysoIP data
1109 from all *Aldh1l1-Cre+* lines compared to one another

1110 **Supplemental Table 4:** Log_2FC and p-values for TMT-MS data for individual mouse LysoIP data
1111 from all *Syn-Cre+* lines compared to one another

1112 **Supplemental Table 5:** Gene ontology analysis of LysoIP proteins significantly altered (*Grn* WT
1113 vs *Grn* KO) in *Syn-Cre+*;*Grn* KO LysoIP samples

1114 **Supplemental Table 6:** Log_2FC and p-values for TMT-MS data for individual mouse, brain
1115 derived LysoIP data from all *Cx3cr1-Cre+* lines compared to one another

1116 **Supplemental Table 7:** Gene ontology analysis of brain-derived LysoIP proteins significantly
1117 altered (*Grn* WT vs *Grn* KO) in *Cx3cr1-Cre+*;*Grn* KO LysoIP samples

1118 **Supplemental Table 8:** Log_2FC and p-values for TMT-MS data for individual mouse, spleen
1119 derived LysoIP data from all *Cx3cr1-Cre+* lines compared to one another

1120 **Supplemental Table 9:** Log_2FC and p-values for TMT-MS data for individual mouse, brain-
1121 derived LysoIP data from all all Cre lines

1122 **Supplemental Table 10:** Log_2FC and p-values for TMT-MS data for individual mouse, brain-
1123 derived LysoIP data comparing log_2FC (vs *Grn* WT) values of *Grn* KO samples between Cre lines

1124